4 Results

4.1 The structure of the TRAPP subunit Tpc6B

4.1.1 Expression and purification of recombinant Tpc6B

The human cDNA encoding for Tpc6B (NCBI accession number CAD61947) was cloned using *Bam*HI / *Not*I restriction enzymes into the bacterial expression vector pQTEV [92]. The resulting plasmid pQTEV-*Tpc6B* was transformed into *E. coli* SCS1 Rosetta and protein was expressed in SB medium containing 100 µg ml^{-1} ampicillin and 34 µg ml^{-1} chloramphenicol for 4 h at 37 °C.

The expressed 7×His-Tpc6B was purified with Ni-NTA resin according to the batch purification protocol (see 3.2.5.1). 10 mM DTT and TEV protease at a ratio 1:20 (w/w) were added to elution fractions; and the reaction was incubated for 48 h at 4 °C. After dialysis against His-lysis buffer, protein was loaded onto a PoRos Talon Superflow column using a Vision Chromatography system. Unbound fractions were collected and loaded on a Superdex 75 (HiLoad, 16/60) column in 20 mM Tris pH 7.4, 100 mM NaCl and 1 mM DTT, and peak fractions were concentrated to 9.7 mg ml^{-1}. The elution volume of Tpc6B was 53 ml, corresponding to a molecular weight of ~40 kDa. Thus dimerization of Tpc6B in solution is observed. After confirming monodispersity with dynamic light scattering the protein was used for crystallization. The recombinant protein contains two additional N-terminal residues (Gly-Ser) that remain from the cleavage site after TEV-protease digestion.

Selenomethionine (SeMet)-labeled Tpc6B was produced in *E. coli* B834 (DE3) [70] and could be purified following the same protocol as for native Tpc6B.

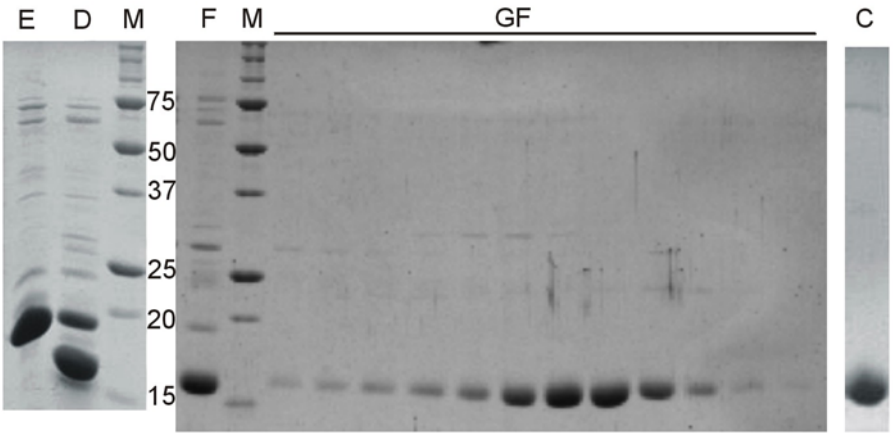

Figure 4.1: SDS-PAGE of samples from the purification of Tpc6B.
E: elution from Ni-NTA batch binding; D: TEV protease digest; F: flowthrough from Ni-Poros chromatography; GF: peak fractions of Superdex 75 gel-filtration; C: concentrated sample used for crystallsation; M: marker lanes; Molecular weight of marker proteins is given in kDa.

4.1.2 Crystallization of Tpc6B

For crystallization trials, purified Tpc6B was tested with the crystal screens Hampton, PEG_Ion, Index_HT and Salt_HT (see appendix B). Experiments were carried out in 96-well format at 20 ºC by the sitting-drop method using a semi-automated dispensing system [74]. Reservoir volume was 400 µl and the droplet contained 400 nl of each, protein solution and precipitant. Good initial crystal were observed after 1 day in conditions that mostly contained 20 or 25% PEG3350 and sulfate salts. In several rounds of fine screening, 22-23% PEG 3350, 0.1 M HEPES pH 7.5, and 0.3 M $(NH_4)_2SO_4$ or 0.4 M Li_2SO_4 were determined to be the best solutions for obtaining Tpc6B crystals, that grew as long plates with dimensions of up to 2 µm x 10 µm x 500 µm. For data collection, crystals were dipped for 30 s into cryo-solution containing additional 10% glycerol and flash frozen in liquid nitrogen.
SeMet-labeled Tpc6B was crystallized under the same conditions.

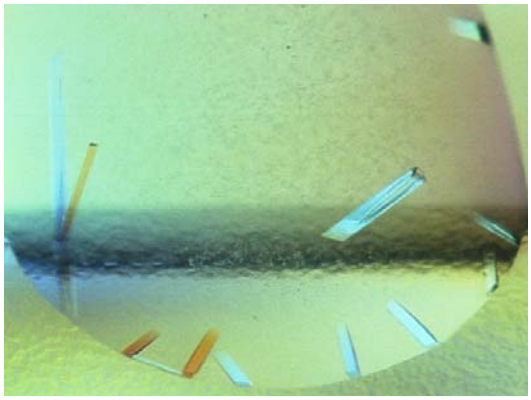

Figure 4.2: Crystals of Tpc6B after 1 day, grown in 22% PEG 3350, 0.4 M Li_2SO_4, 0.1 M HEPES pH 7.5 at 20 °C.

4.1.3 Data collection and structure determination

To determine the optimal wavelength and the atomic scatter factors (Equation 3.12) for anomalous data collection, a fluorescence scan of the SeMet crystal at the selenium edge was performed and evaluated with the program CHOOCH [81]. The results are listed in Table 4.1.

	E (eV)	λ(Å)	*f'*	*f''*
Inflection	12,652.82	0.9799	-10.1	3.0
Peak	12,654.99	0.9797	-7.9	5.0

Table 4.1: Atomic scattering factors of SeMet-Tpc6B crystals at peak and inflection wavelength.

Data from a native crystal to 1.7 Å and a derivative crystal to 1.9 Å resolution were collected at 100 K at the Protein Structure Factory beamlines BL14.1 and BL14.2 of the Free University of Berlin at BESSY (Berlin, Germany, [76]). Data were reduced and scaled using HKL2000 [77]. Data collection statistics are listed in Table 4.2.

	Native Tpc6B	SeMet-Tpc6B
Wavelength [Å]	0.9184	0.9797
Resolution [Å]	50-1.7 (1.76-1.7)	50-1.9 (1.97-1.9)
Space group	C2	C2
Unit cell	a = 99.42 Å b = 57.01 Å c = 60.41 Å β =117.16 °	a = 99.95 Å b = 57.08 Å c = 60.63 Å β = 117.36°
Completeness [%]	98.5 (89.9)	95.1 (60.2)
Mosaicity [°]	0.57-0.4	0.7-0.37
Total reflections	154,444	136,512
Unique reflections	32,829	23,200
$\langle I \rangle / \langle \sigma(I) \rangle$	22.81 (2.27)	9.33 (1.91)
R_{sym} (Equation 3.7)	0.054 (0.475)	0.112 (0.531)

Table 4.2: Data collection statistics for native and SeMet-Tpc6B crystals. Values in parenthesis refer to the outer shell of reflections.

For structure determination of Tpc6B, selenium peak-wavelength data to 2.4 Å resolution were used for single-wavelength anomalous diffraction (SAD) phasing. The Mathews coefficient suggested the presence of two Tpc6B molecules per asymmetric unit. Initial phases were calculated using SOLVE [82], and density modification implemented in RESOLVE [83] was used to improve phases. The initial model comprising 58% of 320 residues per asymmetric unit was automatically built with RESOLVE and gave an *R*-factor of 29%. The model was interactively improved using the program O [85] and refined to R_{work} / R_{free}-factors of 23.3% / 27.5% using REFMAC5 [88].

The model was placed into the isomorphous unit cell of the high-resolution native protein data set. During several rounds of iterative model building and refinement (including TLS groups) the model was extended to 290 residues per asymmetric unit and 5 sulfate ions, 4 glycerol and 126 water molecules were placed in the electron density map, yielding final R_{work} / R_{free}-factors of 17.5% and 20.9% (Table 4.3). The coordinates and diffraction amplitudes were deposited in the Protein Data Bank with accession code 2BJN.

	Native Tpc6B
R_{work} / R_{free} [%] (Equation 3.21)	17.5 / 20.9
rmsd bond distances [Å]	0.018
rmsd bond angles [°]	1.74
mean *B* value [Å^2]	31.5
Ramachandran plot [%] [89]	
Most favored	92.2
Additionally allowed	7.8

Table 4.3: Refinement statistics of the Tpc6B structure.

4.1.4 The structure of Tpc6B

In the crystal, two Tpc6B molecules are present per asymmetric unit, forming a dimer (Figure 4.3a). Each Tpc6B subunit shows an α/β-plait topology defining Tpc6B as member of the (α+β) class of proteins. Five α-helices are arranged on one side of a twisted, antiparallel, four-stranded β-sheet, and a 3_{10}-helix segment comprises the residues Arg100-Leu102. The arrangement of secondary structure elements with regard to the primary structure is shown in Figure 4.6a. Two C-terminal residues and the loop 6 (Thr103-His114) are not visible in the electron density map due to disorder. The root mean square deviation (rmsd) between equivalent C^{α} atoms after a superposition of the two molecules per asymmetric unit with the program LSQKAB [93] is 0.5 Å. There are various differences in the conformation of both monomers, mainly due to different crystal contacts of the chains. In addition, the loop region 2 (Glu51-Glu63) is partially unordered and missing in chain A. Considering the structural variability in these regions, depending on crystal contacts and a large number of disordered side chains, these areas have to be considered flexible in solution and might acquire order upon TRAPP complex formation. Between the helical face and the β-sheet of each chain, a wide depression is found (Figure 4.3a). This region might represent a binding surface for another TRAPP complex subunit.

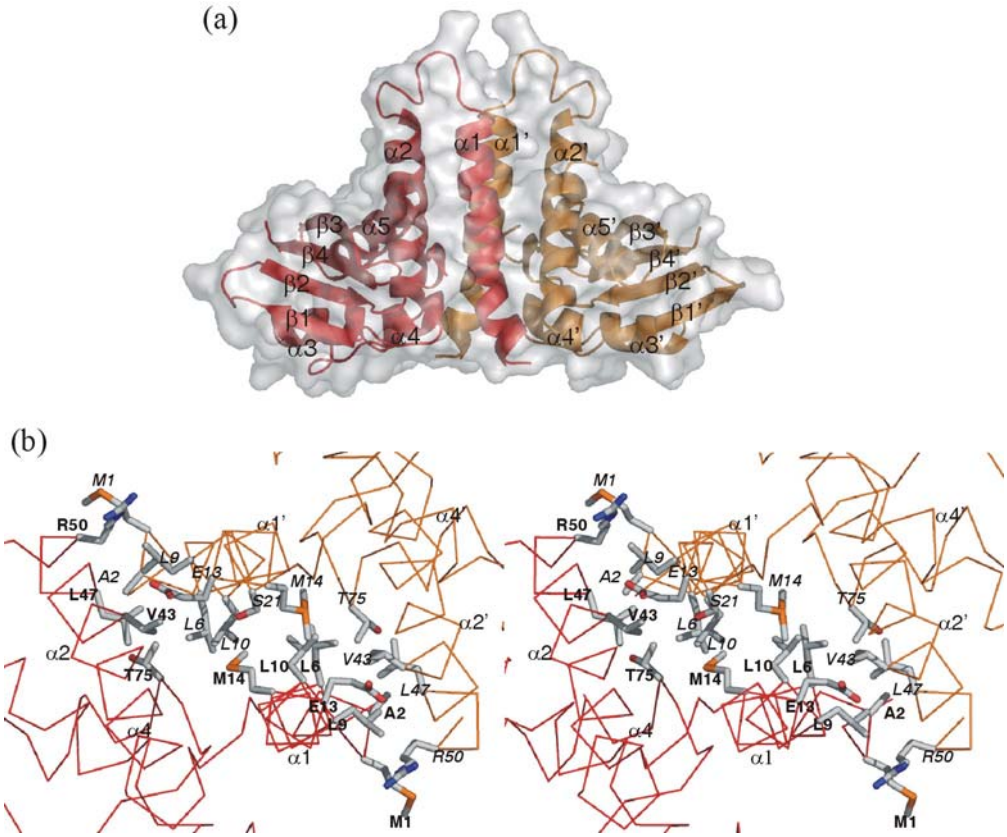

Figure 4.3: (**a**) Cartoon representation of the Tpc6B dimer with a semitransparent surface. The subunits are colored red and orange and secondary structure elements are labeled. (**b**) Stereo image of the Tpc6B interaction interface. For both monomers (colored red and orange) the residues most strongly involved in dimerization are shown. Amino acids from different chains are labeled in bold print and italics, respectively.
Unless stated otherwise, pictures were prepared using PyMOL [4].

Dimerization of Tpc6B occurs *via* the helical face of the protein, through the interaction of the helices α1 and α2 with α1' and α2', respectively, with minor contributions of α4 and α4' (Figure 4.3b). The surface area buried in the dimerization interface covers 2,396 Å^2, corresponding to 15.7% of the total solvent accessible surface area (15,203 Å^2) of both monomers as calculated with XSAE (courtesy Clemens Broger). The contact areas are mainly composed of hydrophobic and van der Waals interactions between aliphatic residues without any buried water molecules. The most prominent residues with a contribution of more than 40 Å^2 to the dimerization interface are Met1, Ala2, Leu6, Leu9, Leu10, Glu13, Met14 (and Ser21 in chain A) in helix α1, Val43, Leu47 and Arg50 in helix α2, and Thr75 in α4.

4.1.5 Structural comparison of Tpc6B and Bet3

The overall structure of Tpc6B resembles strikingly that of Bet3 (Figure 4.4a). In spite of only 17% sequence identity, the superposition over 74% (Tpc6B sequence) of the α-carbon backbones of the monomers of both proteins with LSQKAB [93] shows an rmsd of 1.5 Å. Differ-

ences in structure are mainly confined to the loop regions, whereas the α/β-plait cores of both proteins show little divergence.

A hydrophobic tunnel is located on the α-helical face of Bet3. In the structure of human Bet3 purified from yeast, it could be shown that a palmitic acid covalently bound to the conserved Cys68 occupies this cavity, whereas mouse Bet3 purified from *Escherichia coli* was found to be acylated with a mixture of palmitate and myristate chains [56, 57]. No acylation is observed for Tpc6B, consistent with the absence of an equivalent cysteine. In Tpc6B, the area corresponding to the hydrophobic cavity of Bet3 is entirely closed (Figure 4.4b), due to less space between helices α3/α4 and α5 in Tpc6B. The remaining space is filled with hydrophobic residues, among them four phenylalanines. Tpc6B Phe58 is located at the position of the acylated residue Cys68 in Bet3, thus blocking the channel entrance. The position of Bet3 Ala82 is occupied by Phe72 in Tpc6B. Finally, Tpc6B Phe51, Ile64, Phe67 and Leu134 at the positions of Bet3 Phe59, Thr74, Val77 and Val142 point into the center of the cavity.

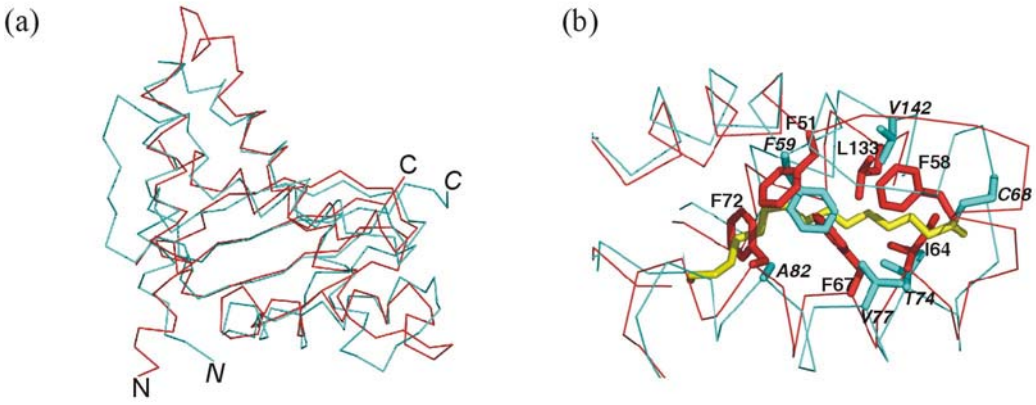

Figure 4.4: Structural comparison of Tpc6B (red) and Bet3 (cyan). (**a**) Superposition of Tpc6B and Bet3 monomers. (**b**) Placement of the palmitate (yellow) from the hydrophobic cavity of Bet3 into the corresponding area of Tpc6B after least-squares superposition of the protein chains. Residues at the corresponding positions of Bet3 are labeled with italics.

Another feature described for Bet3 is a wide and flat dimer surface with a number of positively charged residues. Mutation of some of these basic residues resulted in a loss of Bet3's capacity to associate with membranes [56]. This suggests that the positively charged amino acids mediate membrane association, probably by interacting with the acidic head groups of phospholipids. For comparison of the corresponding faces of Tpc6B and Bet3, potential maps of both proteins were calculated (Figure 4.5a). Tpc6B does not show the flat, positively charged surface strip described for Bet3. The pattern of acidic and basic solvent exposed amino acids yields a rather mixed charge distribution, and the surface is more uneven.

It was therefore interesting to test whether Tpc6B would be able to associate with membranes as it was reported for Bet3 [56, 57]. Total cleared lysate from HEK293 cells overexpressing Bet3 and Tpc6B was subjected to ultracentrifugation. Supernatant (containing cytosol) and pellet (microsomal fraction) were analyzed by SDS-PAGE and Western blot analysis. In these membrane preparations only Bet3, but not Tpc6B was found in microsomal fractions (Figure 4.5b).

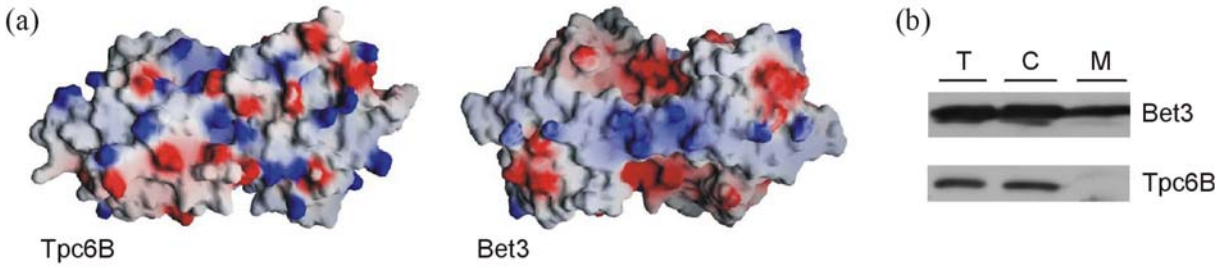

Figure 4.5: (**a**) The putative membrane interacting surfaces of the Tpc6B and Bet3 dimers. An electrostatic potential map calculated with DELPHI [2] is projected onto the molecular surface of the proteins using GRASP [9]. Positive and negative potential is colored blue and red, respectively, at the 10 kT level. (**b**) Membrane preparations of cells expressing myc-Bet3 and flag-Tpc6B. Total cleared lysate (T), cytosolic (C) and microsomal (M, 10-fold concentrated) fractions were analyzed by SDS-PAGE and Western blot with α-myc and α-flag antibodies.

4.2 Studies on the Bet3 protein family

Two common motifs in the amino-acid sequence of Tpc6B, Bet3 and Tpc5 identify these proteins as members of the same protein family within TRAPP. The structural similarity between Tpc6B and Bet3 suggested a closer investigation of the structural and functional relationship between those proteins.

4.2.1 Purification of Bet3 and Tpc5

Bet3 was purified following a modified protocol based on the purification stratgy described in [57]. 6xHis-Bet3-StrepII was expressed with the plasmid pYEXTHSBN-*Bet3* in *S. cerevisiae* AH22*ura*3 (see 3.2.2). The fusion protein was purified by two subsequent affinity chromatographic steps, first with Talon resin (3.2.5.3), followed by binding to Strep-Tactin (3.2.5.4).

The human *Tpc5* cDNA (NCBI accession number AAH42161) was PCR-amplified with *Taq* polymerase from the IMAGE clone p962F0644 with *Esp*3I restriction sites generating *Bam*HI and *Not*I overhangs and cloned into pQTEV [92].

The 7×His-Tpc5 fusion protein was first purified under denaturing conditions (3.2.5.5). Elution fractions were dialysed against buffer containing 6 M urea, 500 mM NaCl, 10% glycerol and 20 mM Tris pH 7.4 and loaded on a HiTrap chelating column (Amersham) charged with Ni(II). Protein was refolded on the column with a 90 min gradient from 6 M urea to 1 M urea and eluted with His-elution buffer.

4.2.2 A common fold for the Bet3 protein family

Considering the high structural similarity between Tpc6B and Bet3, their α/β-plait fold might represent the common fold for all paralogous Bet3 family members, including Tpc5. A sequence alignment of the human proteins Tpc6B, Tpc5 and Bet3 (Figure 4.6a) shows that conserved and similar residues between different family members are predominantly located in the α-helical secondary structure elements. Major variations in length and conservation of the primary structure are only found in loop regions. In addition, the proteins differ in the length and sequence of their N- and C-termini. The highest similarity is found for two motifs (LX_2#GX_2#GX_2LXE and G#$_2$XGXL) that have been previously described for the yeast Bet3 family members [39]. These motifs are mostly conserved in the human proteins as well, and they are located in the interior of the proteins in helices α2 and α5.

To test the hypothesis of a common family fold, all three proteins were purified and characterized by circular dichroism (CD) spectroscopy (Figure 4.6b). The shapes of the CD spectra are

similar, indicating a similar composition in secondary structure. Differences are observed in the amplitudes of the spectra, which can be explained with the different ratio of core region with similar secondary structure to unordered loop and terminal regions for Tpc6B and Bet3. Considering the primary structure of Tpc5 which is more similar to Bet3 in the length of putative disordered regions, it is not surprising that its CD spectrum resembles the Bet3 spectrum more than that of Tpc6B.

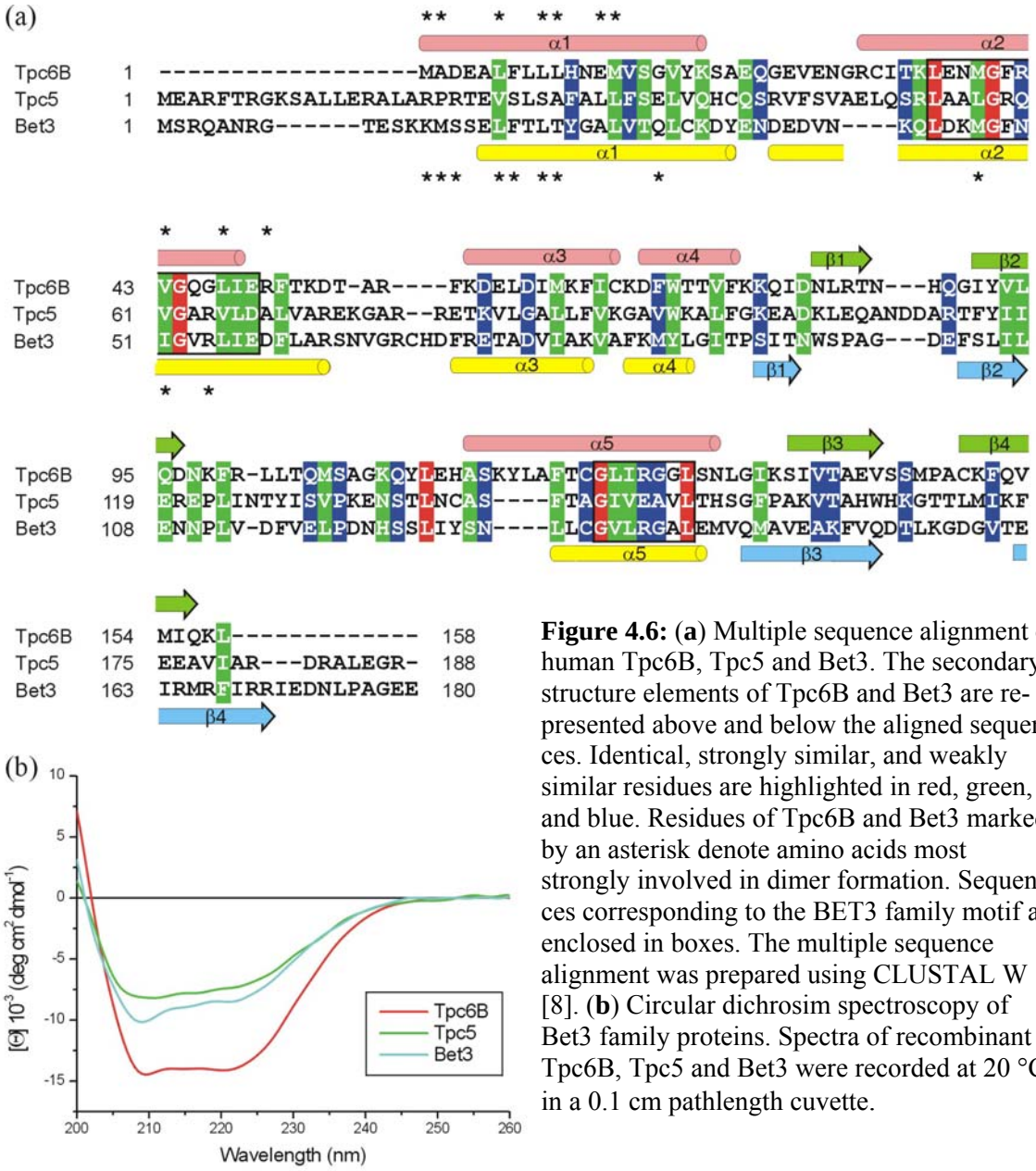

Figure 4.6: (**a**) Multiple sequence alignment of human Tpc6B, Tpc5 and Bet3. The secondary structure elements of Tpc6B and Bet3 are represented above and below the aligned sequences. Identical, strongly similar, and weakly similar residues are highlighted in red, green, and blue. Residues of Tpc6B and Bet3 marked by an asterisk denote amino acids most strongly involved in dimer formation. Sequences corresponding to the BET3 family motif are enclosed in boxes. The multiple sequence alignment was prepared using CLUSTAL W [8]. (**b**) Circular dichrosim spectroscopy of Bet3 family proteins. Spectra of recombinant Tpc6B, Tpc5 and Bet3 were recorded at 20 °C in a 0.1 cm pathlength cuvette.

4.2.3 Interaction of Tpc6B and Bet3

In the crystal structure of Tpc6B, two molecules form a dimer with subunits related by a non-crystallographic dyad axis. The dimerization of Bet3 occurs at a two-fold crystallographic axis. Nevertheless, dimerization of both proteins occurs in a similar manner. The intermolecular interactions are mostly mediated by hydrophobic interactions of aliphatic residues located on the helices α1, α2, and with less contribution α4. The similarities in the dimerization surfaces of both proteins leads to the intriguing possibility of a hetero-dimerization between Tpc6B and Bet3.

A direct interaction between Tpc6B and Bet3 could be proven with association studies. The Tpc6B:Bet3 interaction can be shown *in vivo* by co-immunopreciptation of myc-Bet3 with flag-Tpc6B (Figure 4.7a). The stoichiometry of the Tpc6B:Bet3 interaction was determined with crosslinking experiments using recombinant proteins (Figure 4.7b). Homodimer formation of both proteins in solution could be shown when they were crosslinked with glutaraldehyde separately. An equimolar mixture of Tpc6B and Bet3 led to the formation of a crosslinking product of intermediate size which was confirmed to contain both proteins using mass spectrometry. Based on these data and the crystal structures, a model for a putative TRAPP subcomplex could be derived, where Tpc6B and Bet3 form heterodimers, utilizing their closely similar dimer interfaces (Figure 4.7c).

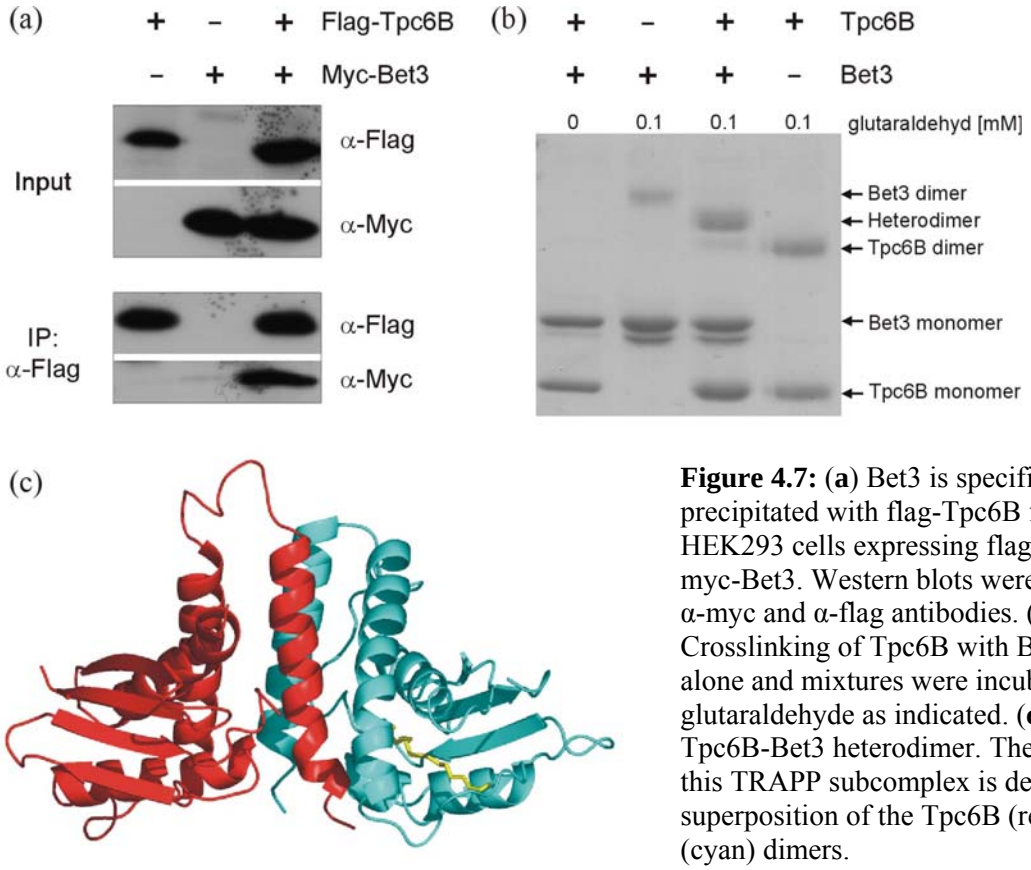

Figure 4.7: (**a**) Bet3 is specifically co-precipitated with flag-Tpc6B from HEK293 cells expressing flag-Tpc6B and myc-Bet3. Western blots were probed with α-myc and α-flag antibodies. (**b**) Crosslinking of Tpc6B with Bet3. Proteins alone and mixtures were incubated with glutaraldehyde as indicated. (**c**) Model of a Tpc6B-Bet3 heterodimer. The structure of this TRAPP subcomplex is derived from a superposition of the Tpc6B (red) and Bet3 (cyan) dimers.

4.2.4 Tpc5 interacts with Bet3, but not Tpc6B

The putative similar fold of the three Bet3 family proteins leads to the hypothesis that Tpc5 might also form homodimers or heterodimers with Bet3 and Tpc6B.

In crosslinking studies, homodimer formation of Bet3 and Tpc6B could be shown, but no Tpc5 dimers were observed under these conditions (Figure 4.8a). When co-expressed in HEK293, Tpc5 could be co-immunoprecipitated with Bet3 (Figure 4.8b). In a His-pulldown assay the interaction of Tpc5 and Bet3, expressed separately in HEK293 cells, with recombinant Tpc6B was probed. Whereas the *in vivo* interaction of Tpc6B and Bet3 (Figure 4.7a) could be verified with this *in vitro* system, no association of Tpc6B with Tpc5 was observed (Figure 4.8c). These data indicate that Tpc5 might form a heterodimer with Bet3, but no homodimers, and does not associate with Tpc6B.

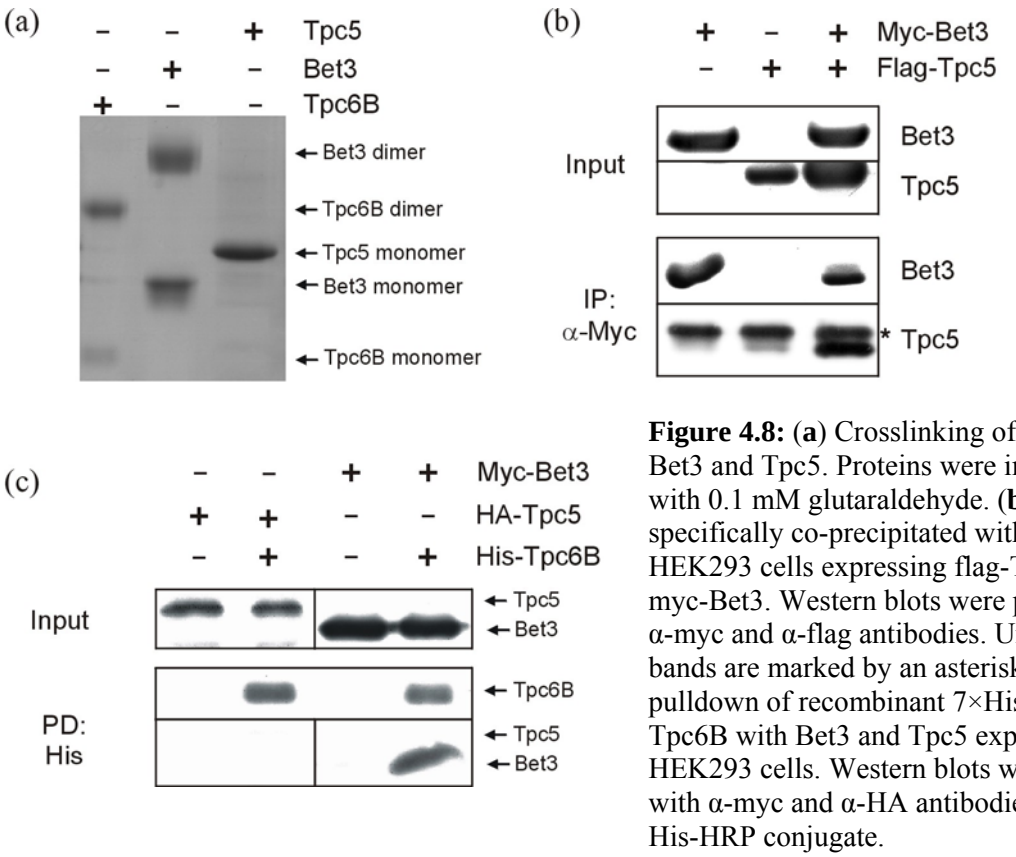

Figure 4.8: (**a**) Crosslinking of Tpc6B, Bet3 and Tpc5. Proteins were incubated with 0.1 mM glutaraldehyde. (**b**) Tpc5 is specifically co-precipitated with Bet3 from HEK293 cells expressing flag-Tpc5 and myc-Bet3. Western blots were probed with α-myc and α-flag antibodies. Unspesific bands are marked by an asterisk. (**c**) His-pulldown of recombinant 7×His-tagged Tpc6B with Bet3 and Tpc5 expressed in HEK293 cells. Western blots were probed with α-myc and α-HA antibodies and α-His-HRP conjugate.

4.3 The structure of the Bet3:Tpc6B subcomplex of TRAPP

After the determination of the crystal structures of Bet3 and Tpc6B homodimers, the crystallization of the heterocomplex of both proteins was pursued. This would ultimately prove the model postulated based on the structural and biochemical data and provide new information on the TRAPP complex assembly.

4.3.1 Expression and purification of the Bet3:Tpc6B heterodimer

The human *Bet3* cDNA (NCBI accession number AF041432) was cloned between the *Bam*HI and *Not*I restriction sites of the multiple cloning site (MCS) I of the bacterial expression vector pETDuet-1. The human *Tpc6B* (NCBI accession number CAD61947) cDNA was amplified with *Nde*I and *Xho*I restriction sites and cloned into the MCS II of pETDuet-*Bet3*. Mutants were generated using the QuikChange™ mutagenesis.

E. coli BL21 (DE3) cells were transformed with the resulting plasmids pETDuet-*Bet3:Tpc6B* and expressed in LB medium containing 100 µg ml^{-1} ampicillin. 6×His-Bet3:Tpc6B was purified with Ni-NTA agarose according to the batch binding protocol (see 3.2.5.1). The elution fractions were loaded on a Superdex 75 (HiLoad, 26/60) column equilibrated with 25 mM Tris pH 7.4, 250 mM NaCl and 5 mM β-mercaptoethanol, and peak fractions were concentrated to ~13 mg ml^{-1}.

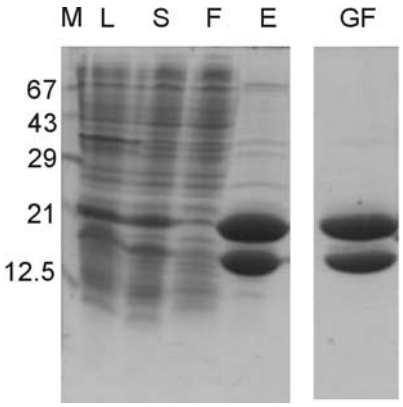

Figure 4.9: SDS-PAGE monitoring of a Bet3:Tpc6B preparation.
L: total cell lysate; S: soluble supernatant after centrifugation; F: flowthrough after batch binding E: elution from Ni-NTA matrix; GF: purfied sample after Superdex 75 gel-filtration; M: marker lanes; Molecular weight of marker proteins is given in kDa.

4.3.2 Crystallization of 6×His-Bet3:Tpc6B

After confirming monodispersity with dynamic light scattering, the protein complex was used for crystallization trials applying the crystal screens Hampton, PEG_Ion, Index_HT and Salt_HT (see appendix B). Experiments were carried out in 96-well format at 20 ºC by the sitting-drop method using a semi-automated dispensing system [74]. Reservoir volume was 400 µl and the droplet contained 400 nl of each protein solution and precipitant. Best crystals were obtained in 18%-20 % PG3350, 0.2 M tri lithium citrate (Figure 4.10a). One crystal was

readily washed in reservoir solution, loaded onto an SDS-PAGE gel and proteins were detected *via* silver staining (Figure 4.10b). The presence of both proteins in the crystal could be confirmed. Crystals were flash-frozen in liquid nitrogen with additional 5% glycerol as cryoprotectant.

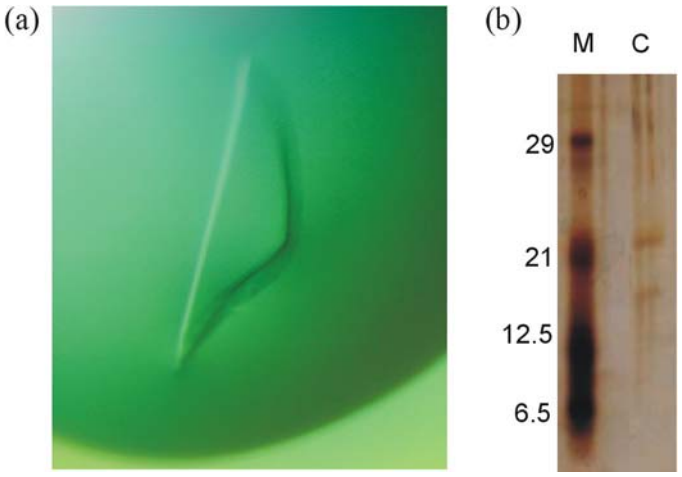

Figure 4.10: (**a**) Crystal of the Bet3:Tpc6B complex, grown in 20% PEG 3350, 0.2 M tri lithium citrate. (**b**) Silver-stained SDS-PAGE gel of a Bet3:Tpc6B crystal. C: washed crystal; M: marker lanes; Molecular weight of marker proteins is given in kDa.

4.3.3 Structure determination of Bet3:Tpc6B with molecular replacement

Data from a single crystal were collected at 100 K at the Protein Structure Factory beamline BL14.2 of the Free University of Berlin at BESSY (Berlin, Germany, [76]). Data were processed and scaled using XDS and XSCALE [78] to 2.3 Å resolution (Table 4.4).

	Bet3:Tpc6B
Wavelength [Å]	0.9537
Resolution [Å]	20-2.3 (2.44-2.3)
Space group	C2
Unit cell	a = 69.45 Å b = 69.59 Å c = 144.01 Å β = 91.55°
Completeness [%]	95.6 (90.1)
Total reflections	101,609 (15,482)
Unique reflections	29,365 (4,470)
$\langle I \rangle / \langle \sigma(I) \rangle$	13.76 (3.7)
R_{sym} (Equation 3.7)	0.054 (0.344)

Table 4.4: Data collection statistics for Bet3:Tpc6B crystals. Values in parenthesis refer to the outer shell of reflections.

Initial phases were obtained by molecular replacement using MOLREP [84], with Bet3 and Tpc6B monomers as search models. Two positions for each monomer were identified, revealing the presence of two heterodimers per asymmetric unit. The initial model yielded R_{work} / R_{free} factors of 45.9% / 47.4% after rigid body refinement and 28% / 42% after restrained refinement with REFMAC5 [88]. After two rounds of automated model building with ARP/wARP [87] and including non-crystallographic symmetry in the refinement, *R*-factors dropped to 27.4% / 36.2%. Initial rounds of model building with O [85] and refinement using REFMAC5 were followed by simulated annealing performed with CNS [94] to reduce model bias (giving R_{work} / R_{free} 23.9% / 30.9%). To refine the palmitoylated cysteine residue of Bet3, a library for REFMAC5 was generated using the PRODRG server [95]. During several rounds of iterative model building and refinement (including TLS) the model was extended to 680 residues per asymmetric unit. 57 water molecules found with ARP/wARP [87] were placed in the electron density map, leading to final *R*-factors of 22.1% and 26.9% (Table 4.5). The coordinates and diffraction amplitudes were deposited in the Protein Data Bank with accession code 2CFH.

	Bet3:Tpc6B
R_{work} / R_{free} [%] (Equation 3.21)	22.1 / 26.9
rmsd bond distances [Å]	0.017
rmsd bond angles [°]	1.55
mean *B* value [Å^2]	56.3
Ramachandran plot [%] [89]	
Most favored	88.6
Additionally allowed	10.4
Generously allowed	1.1

Table 4.5: Refinement statistics of the Bet3:Tpc6B structure.

4.3.4 Structure of the Bet3-Tpc6B complex

In the crystal, two heterodimers are present per asymmetric unit. Each Bet3 and Tpc6B molecule shows the α/β-plait topology described as Bet3 family fold before (Figure 4.11a-c). For Bet3, residues 15-175 and a palmitoyl group covalently attached to Cys68 could be built into the electron density. The Tpc6B model comprises residues 2-104 and 111-157. The root-mean-square deviation of the protein main chains in the heterodimer compared to the subunits as present in homodimer structures is 1.2 Å for Bet3 and 2.4 Å for Tpc6B (LSQKAB, [93]). These conformational differences result from the readjustment of helices α1 and α2 to allow heterodimer formation. The interaction of Bet3 and Tpc6B thus occurs through the same

interface that was observed for the homodimers, mainly by hydrophobic interactions. The buried surface area calculated with the PISA server [96] comprises 2380 Å² and is smaller than the buried surface in the Bet3 (3012 Å²) and similar to that of Tpc6B (2369 Å²) homodimers.

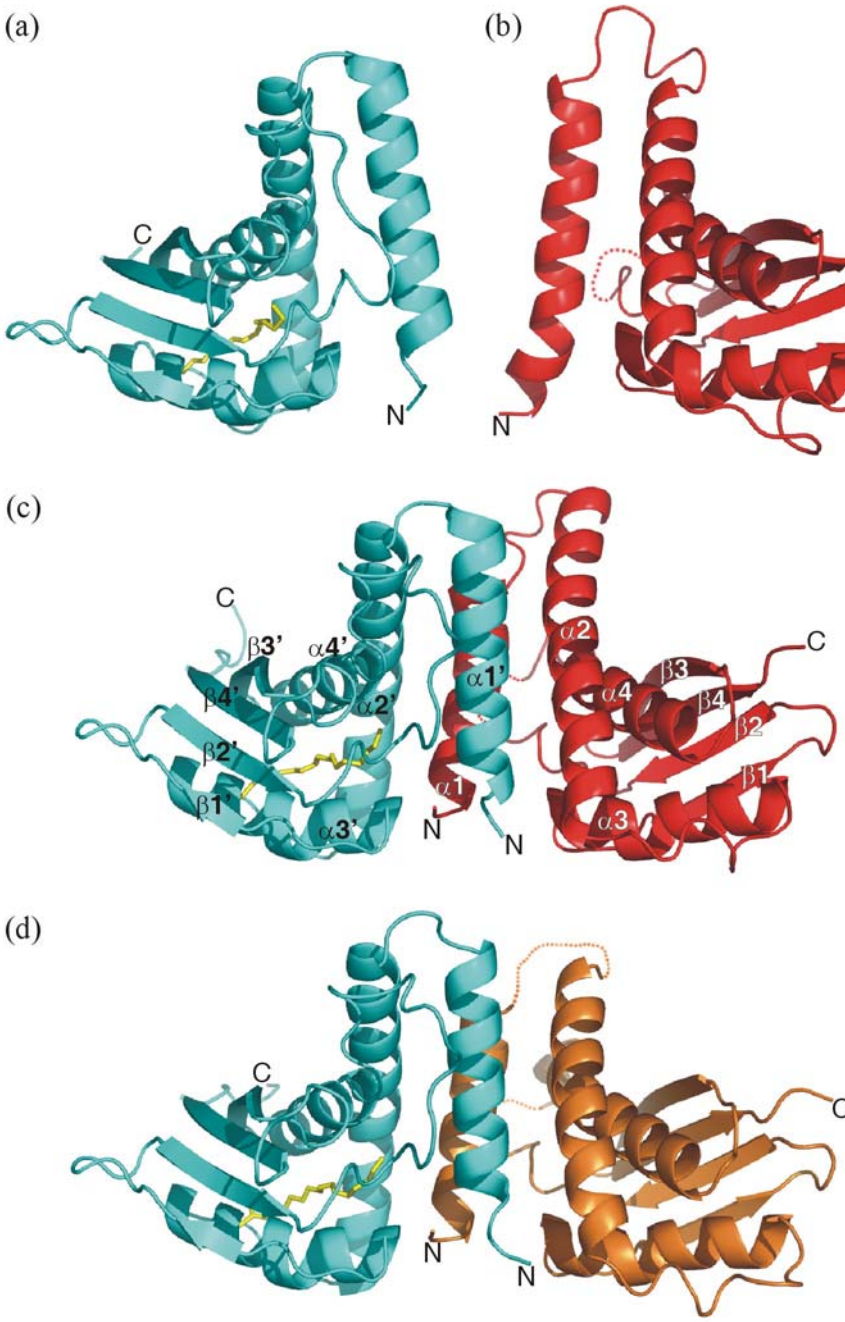

Figure 4.11: Structure of the Bet3:Tpc6 complex. (**a**) Bet3 and (**b**) Tpc6B monomers as they are observed in the homodimer crystal structures are shown in comparison to (**c**) Bet3:Tpc6B with labeled secondary structure elements and (**d**) the Bet3:Tpc6A heterodimer. The structures were superimposed and are depicted in the same orientation. Tpc6B is colored red, Tpc6A orange, and Bet3 cyan with the covalently attached palmitoyl group shown in yellow.

The preference for heterodimerization might be explained by more polar contacts that are formed in the heterodimer, of which a salt bridge between Bet3 Arg62 and Tpc6B Asp3 is the most prominent. In addition, Tpc6B Ala2 is involved in backbone hydrogen bonding with Ser16 and Tyr86 of Bet3. Further polar contacts of Bet3 with Tpc6B are between Asn50 and Glu13, between Gln29 and Arg42 mediated by a water molecule and between Asp33 of Bet3

and Lys35 and Tyr19 of Tpc6B. In contrast, one polar interaction between Glu13 and Arg42 is observed in the Tpc6B homodimer, and in the Bet3 homodimer only Asp33 and Gln29 are involved in intermolecular hydrogen bonding. These polar interactions seem to be responsible for a stabilization of the heterodimer compared with the homodimers as seen with the co-expression of Bet3 and Tpc6 which favored the formation of heterocomplexes.

The overall architecture of the complex is in good agreement with the model that was proposed for the Bet3:Tpc6B complex before (Figure 4.7c) and also resembles the structure of a Bet3:Tpc6A complex published recently [97] by others (Figure 4.11d). The rmsd between 279 of 300 C^{α} atoms visible in both Bet3-Tpc6 isocomplex structures is 0.9 Å. The buried surface area of Bet3:Tpc6A comprises 2475 Å² and is somewhat larger than that of Bet3-Tpc6B. Tpc6A is also engaged in polar interactions with Bet3 that cannot be formed in homodimeric complexes, including the conserved salt bridge between Asp3 and Arg62.

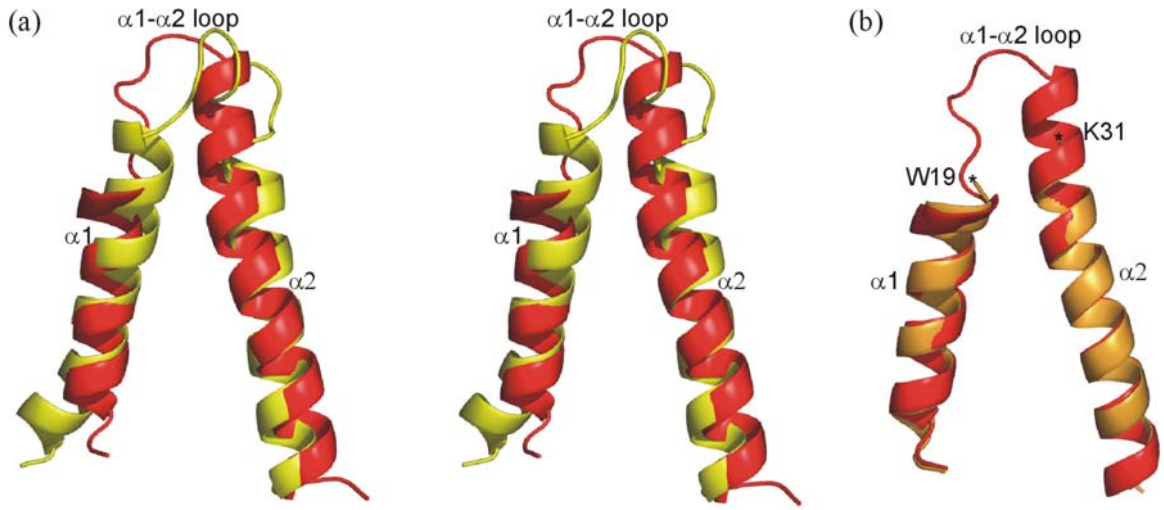

Figure 4.12: (**a**) Stereo picture of the Tpc6B interaction interface. Helices α1 and α2 and the connecting loop region of homodimeric Tpc6B (yellow) and Tpc6B in the heterodimer (red) were superimposed. In the heterocomplex the α1-α2 loop adopts a different conformation and helix α1 is shorter, whereas α2 is elongated. (**b**) Superposition of α1 and α2 of Tpc6A (orange) and Tpc6B (red). The connecting loop between W19 and K31 of Tpc6A, marked by asterisks, is missing in the model.

New structural insight from the Bet3:Tpc6B structure is provided by the examination of the loop connecting helices α1 and α2 of Tpc6B. The superposition of the corresponding areas from the heterocomplex and the Tpc6B homodimer shows a profound structural rearrangement (Figure 4.12a). Helix α1 is shorter and α2 is elongated in the complex structure and the α1-α2 loop adopts a different conformation. As a consequence, the cysteine residue 32 which is located in the interior of the protein in the Tpc6B homodimer becomes solvent accessible. In the crystal that Cys32 is found to be oxidized to sulfenic acid, probably as a result of its exposure to the solvent. Although the α1-α2 loop is not visible in the structure of Tpc6A, the

helices α1 and α2 superimpose nicely with those of Tpc6B in the heterocomplex, also showing a short α1 and a long α2 helix (Figure 4.12b). This observation indicates that the α1-α2 loop regions of both Tpc6 paralogs adopt a similar structural arrangement.

4.3.5 Mum2 binding to the Bet3:Tpc6B heterodimer

The comparison of the homodimer and the heterodimer structures of Bet3 and Tpc6B showed that the α1-α2 loop of Tpc6B is the only part undergoing a prominent structural change upon heterodimer complex formation (Figure 4.12a). A deep groove is formed in the Bet3:Tpc6B heterocomplex that is not present in the homodimeric structures. It can be speculated that this region represents the interaction site for a further TRAPP subunit (Figure 4.13a).

Pulldown experiments showed that the yeast proteins Bet3p and Trs33p, when co-expressed, are able to associate with Bet5p [97]. We asked the question whether this interaction is also observed for the human orthologs Bet3, Tpc6B and Mum2 and how it might be mediated. Using the His-pulldown (3.4.3) assay it was first checked whether one of the complex subunits is responsible and sufficient for Mum2 binding. Only the heterodimeric complex, but not homodimers of Tpc6B or Bet3 are able to bind Mum2 (Figure 4.13b). This result suggests that the putative binding groove of Bet3:Tpc6B could be involved in the association with Mum2.

To test this hypothesis, two mutants of the Bet3:Tpc6B complex were generated. In the 'chimera' mutant, the α1-α2 loop of Tpc6B (Lys20-Cys32) is replaced by the corresponding part of Bet3 (Cys31-Val40). In the 'scrambled' mutant, two residues of Tpc6B facing the groove are mutated (R31E, C32L) as well as three conserved amino acids in the Bet α1-α2 loop (D33K, Y34V, E35R). The complexes could be purified with a single affinity tag, indicating that heterodimerisation of the mutants was intact. The preparation of Bet3:Tpc6B 'scrambled' complex contains more Bet3 than that of the other heterocomplexes. However, the resulting presence of a small Bet3 homodimer fraction should not have a dramatic effect on Mum2 binding.

Interestingly, the 'scrambled' mutant failed to bind Mum2, whereas the 'chimera' mutant is still able to interact with Mum2 (Figure 4.13b). This indicates that Tpc6B α1-α2 loop region does not contribute specific side-chain interactions for Mum2 association, as its replacement did not abolish binding. However, the disruption of the Mum2 interaction in the scrambled mutant points towards a role of the three conserved residues Asp32, Tyr33 and Glu35 of Bet3 for specificity of binding. Since Bet3 homodimers do not bind Mum2, additional contributions of Tpc6B must be required, that are not identified with these experiments.

Taken together, these data indicate that the α1-α2 regions of Bet3:Tpc6B might be involved in the interaction with Mum2. Alternatively, the 'scrambled' mutations might induce local structural rearrangement that interferes with Mum2 binding.

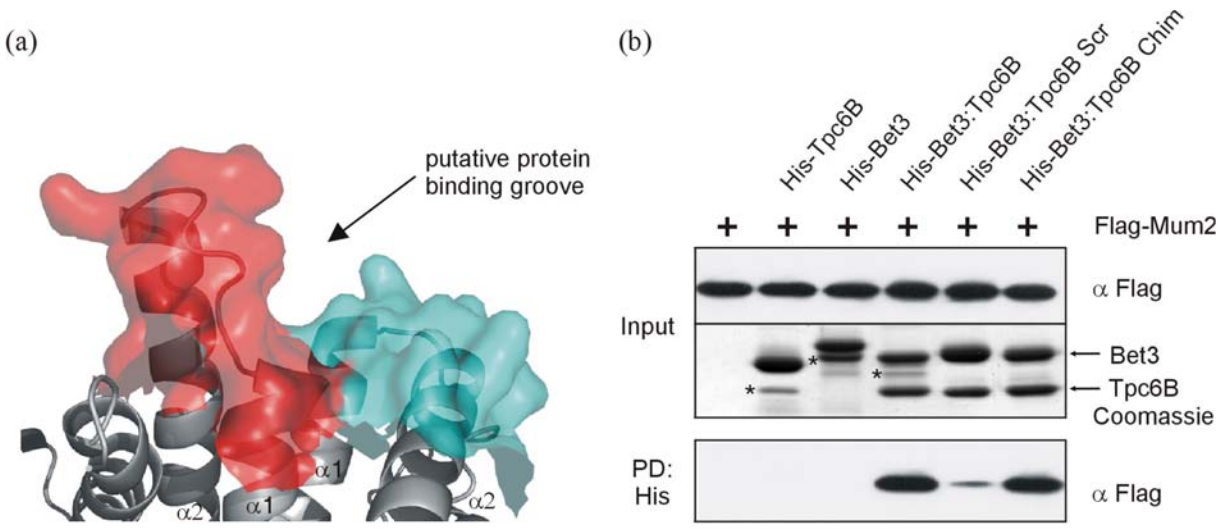

Figure 4.13: (a) Semitransparent surface representation of the α1-α2 loop region of the Bet3:Tpc6B heterodimer that might represent a binding pocket. (**b**) His-pulldown of Mum2 with recombinant His-tagged Tpc6B, Bet3, Bet3:Tpc6B complex and mutants (Scr: Tpc6B R31E,C32L; Bet3 D33K,Y34V,E35R; Chim: α1-α2 loop of Tpc6B replaced by corresponding Bet3 loop). Degradation products are marked by an asterisk. Differences in gel mobility between homo- and heterodimeric preparations are due to expression from different vectors.

4.4 Two variants of Tpc6 are identified in some organisms

The crystal structures of the Bet3:Tpc6A complex [97] and the Bet3:Tpc6B complex presented here show that both Tpc6 paralogs are in principle capable of forming a TRAPP subcomplex. This observation raises the question why two Tpc6 variants are found in some organisms and what their role might be.

4.4.1 A hydrophobic surface patch is conserved between Tpc6 homologs

With a data bank search, one Tpc6 homolog each was identified in *Saccharomyces cerevisiae* (Trs33p), *Arabidopsis thaliana*, *Drosophila melanogaster*, *Caenorhabditis elegans*, *Xenopus tropicalis* and *Gallus gallus*. Two variants are found in mice and humans, with an identity / similarity of about 56% / 85% and 55% / 75%, respectively, between Tpc6A and Tpc6B within one species. Across species, Tpc6B shares higher sequence similarity with its homologs than Tpc6A (Table 4.6). Interestingly, two variants are also found in zebrafish which are both more closely related to Tpc6B and which were thus termed Tpc6B1 and Tpc6B2. This observation indicates that duplications of the Tpc6 gene might have occurred independently during evolution at different points. However, the full genome sequences of e.g. chicken and frog are not yet available. They might fill the gap in the phylogenetic tree between zebrafish and man.

Sequence identity [%]	Tpc6A	Tpc6B
H. sapiens A / B	100 / 56	56 / 100
M. musculus A / B	83 / 55	55 / 97
X. tropicalis	56	67
G. gallus	54	94
D. rerio B1 / B2	56 / 56	83 / 71
D. melanogaster	44	53
C. elegans	49	48
A. thaliana	39	47
S. cerevisiae	30	38

Table 4.6: Sequence conservation of Tpc6A and Tpc6B. Sequences of different Tpc6 paralogs and orthologs were compared using BLAST alignments [98]. The percentages of sequence identity are listed in this table, showing better conservation of Tpc6B compared to Tpc6A.

A CLUSTAL W [8] multiple alignment of Tpc6 sequences from different species leads to the identification of conserved regions in the primary structure (Figure 4.14a). This result is virtually independent of whether Tpc6A, Tpc6B or both are included in the alignment. Surprisingly, the dimer interface does not show significant conservation. Instead, two conserved motifs are located in α2 and α4, respectively. They were described before as Bet3 family motifs [35] also found in the Tpc5 and Bet3 proteins and map to the interior of the protein where they are thought to be involved in the Bet3 family fold formation (4.2.2).

A third region of high conservation is found in a 35 amino-acid stretch covering helix α3 and the strands β1 and β2. The identical and strongly similar residues form a patch with two prominent depressions on the 'back' face of Tpc6B, opposing the interaction interface (Figure 4.14b). An electrostatic potential calculation shows that two hydrophobic pockets are created (Figure 4.14c), which might represent a binding interface for a further TRAPP binding partner. Because the conserved patch is accessible in the homodimer structure of Tpc6B as well and considering that Tpc6B alone did not bind Mum2, that surface region is unlikely to be responsible for Mum2 binding. Instead it is interesting to note that applying the model of membrane association of Bet3 onto the heterodimer, the conserved patch of Tpc6 is likely to face towards the membrane and could thus be involved in membrane association of TRAPP.

Figure 4.14: (**a**) Multiple sequence alignment of Tpc6 orthologs and paralogs. The secondary structure elements of human Tpc6B from the heterocomplex are shown above the aligned sequences. Identical and strongly similar residues are highlighted in green and yellow, and the Bet3 family motifs are indicated. (**b**) View on the conserved surface patch of Tpc6B. Bet3 is colored cyan and Tpc6B red, with identical and similar residues of Tpc6B highlighted green and yellow. Residues forming the surface of the conserved patch are labeled. (**c**) Electrostatic potential map on the protein surface in the same orientation as in (b). Positive and negative potential is colored blue and red, respectively, at the 7 kT level, revealing two uncharged pockets labeled P1 and P2.

Figure on next page.

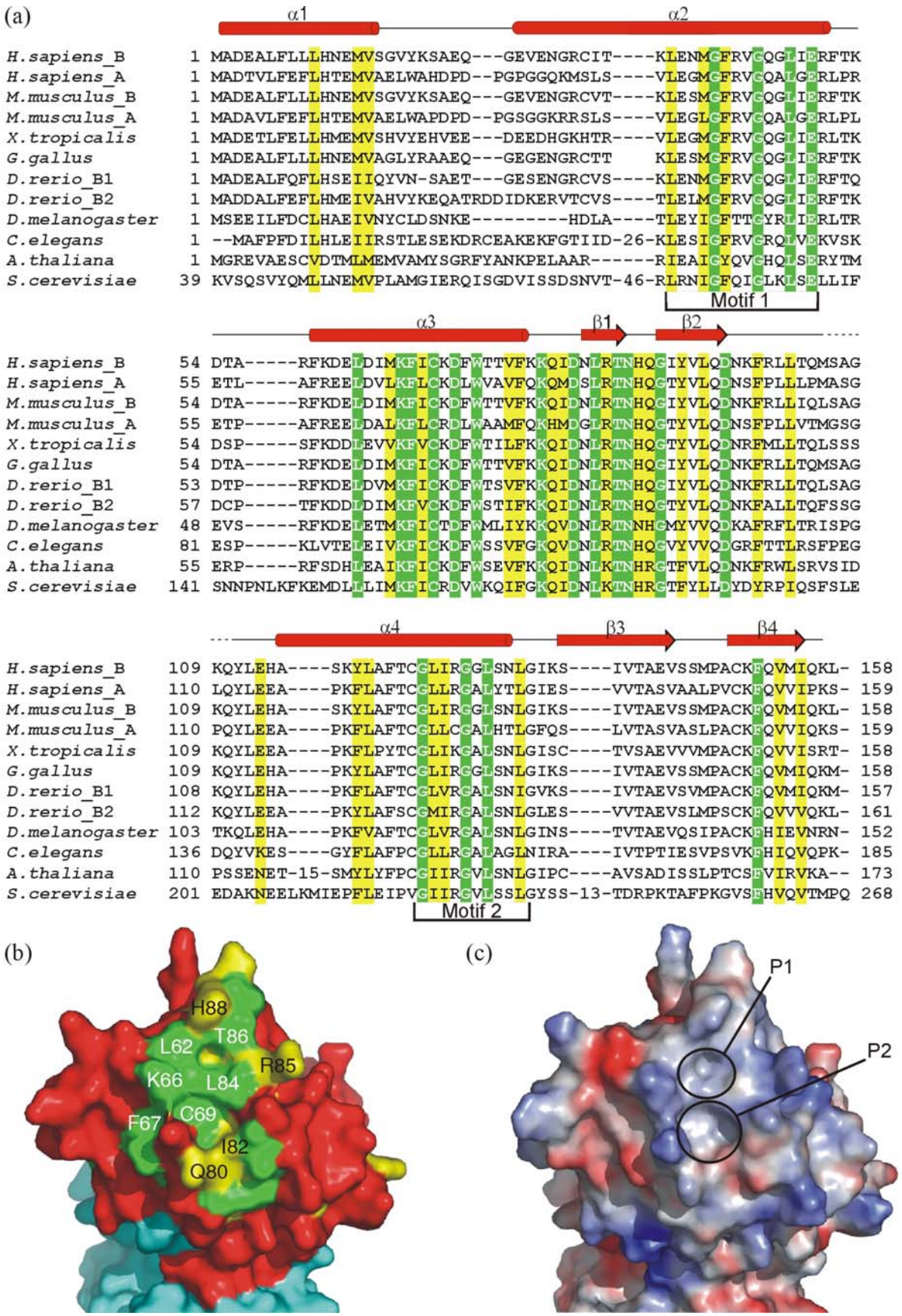

Figure legend on previous page.

4.4.2 Functional comparison of both Tpc6 paralogs

To elucidate possible functions of the two Tpc6 variants, experiments were conducted addressing the interaction with the human TRAPP subunit Mum2 and the mRNA expression level of the proteins in different mouse organs. For this purpose, human *Tpc6A* (NCBI accession number NP_077013; splice variant with 14 additional amino acids in loop α1-α2) cDNA was amplified with *Nde*I and *Xho*I restriction sites using PCR, restriction digested and ligated into the MCS II of pETDuet-*Bet3*. With the resulting plasmid, the His-Bet3:Tpc6A complex was expressed und purified as described for His-Bet3:Tpc6B (see 4.3.1).

As shown above, the Bet3:Tpc6B complex but not Bet3 and Tpc6B alone can bind to Mum2 (see 4.3.5). A pulldown assay was used to test whether both of the Bet3-Tpc6 complexes associate with Mum2. Purified 6×His-Bet3:Tpc6A and 6×His-Bet3:Tpc6B were bound to Talon beads and incubated with the lysate from HEK293 cells expressing flag-Mum2 (Figure 4.15a). Both heterocomplexes specifically bound Mum2 and should thus be able to participate in TRAPP complex formation.

A possible explanation for the existence of two protein isoforms would be a tissue specific expression pattern of both genes. In a quantitative real time polymerase chain reaction (RT-PCR) study, the mRNA levels of *bet3*, *tpc6a* and *tpc6b* in different mouse organs were determined (Figure 4.15b). The expression levels of the TRAPP genes normalized to GAPDH show only minor differences between the investigated tissues. Interestingly, all organs show the same relative expression pattern of *bet3*, *tpc6a* and *tpc6b*. This does not suggests any tissue specificity of *tpc6a* and *tpc6b* in mice. Compared to *tpc6a*, *tpc6b* is expressed at 2-3 fold higher levels in every organ investigated, whereas *bet3* was expressed at intermediate levels. Although the relative copy numbers of RNA are not necessarily reflected in tissue concentrations of protein, these data indicate that both paralogs will be expressed in cells, with probably a moderate abundance of *tpc6b*.

In Figure 4.15c, the residues not conserved between Tpc6A and Tpc6B are mapped onto the surface of the Bet3:Tpc6B heterodimer. Besides single scattered residues, two regions of higher variability between the isoforms are apparent, located in the N-terminal part of helix α1 and the α1-α2 loop region. These patches might mediate distinct functions of the Tpc6 paralogs.

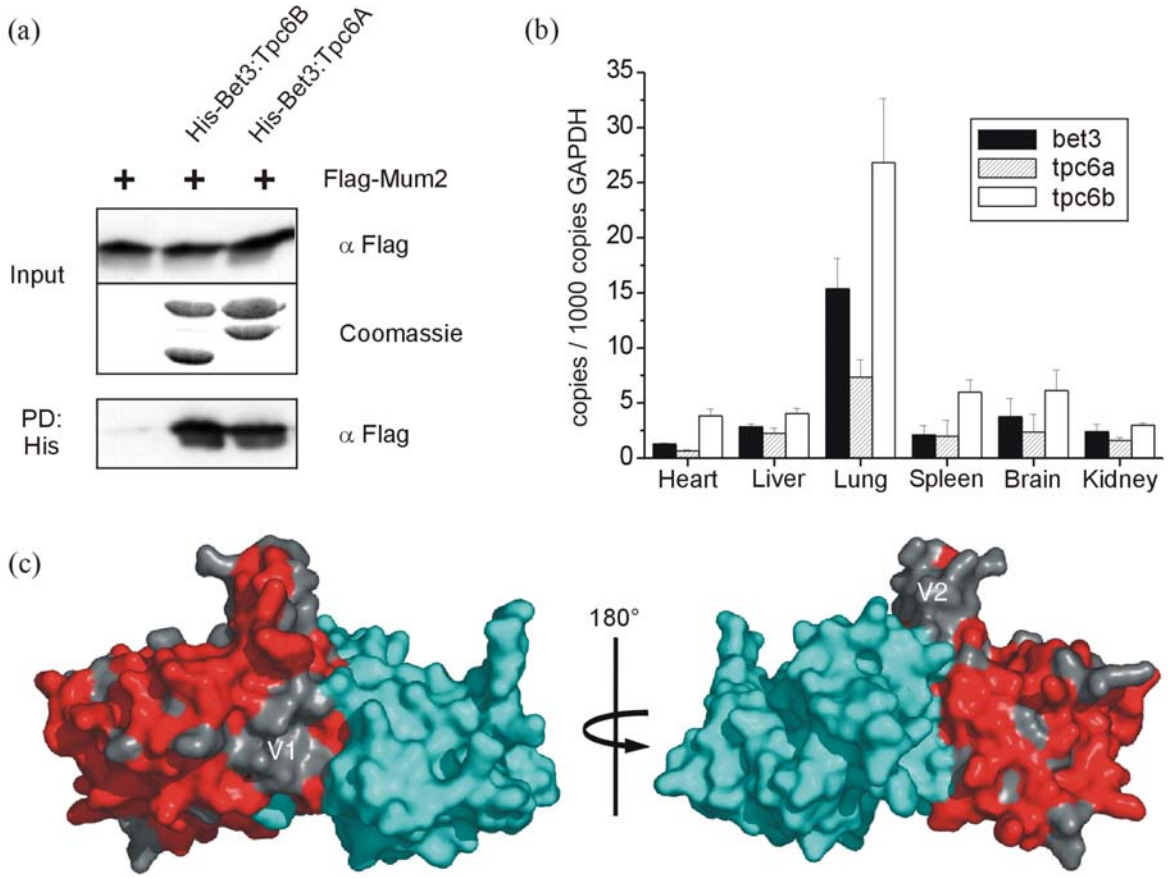

Figure 4.15: (**a**) Pulldown assay with Mum2 and recombinant His-Bet3:Tpc6A and His-Bet3:Tpc6B. Both complexes specifically bind to Mum2. (**b**) Quantitative RT-PCR from different mouse organs shows higher expression levels of *tpc6b* compared to *tpc6a*. The same expression pattern is observed for *bet3* and the *tpc6* paralogs in every organ investigated. Copy numbers relative to GAPDH are given with standard error of mean. (**c**) Surface representation of the Bet3:Tpc6B heterodimer colored as before with residues of Tpc6B different from Tpc6A shown in gray. Two variable regions (V1 and V2) are labeled.

4.5 Identification and characterization of TRAPP subcomplexes

Besides Bet3, Tpc6B and Sedl [55-57, 99], TRAPP subunits were difficult to handle when expressed alone. Therefore, the most promising way to a further characterization of TRAPP would be the reconstitution of subcomplexes by co-expression of subunits. The major focus was put on the Mum2 protein that is known to interact with the Bet3:Tpc6B complex and could also be expressed and purified under defined conditions.

4.5.1 Purification and characterization of Mum2

Because no soluble expression could be achieved for His-tagged Mum2 fusion proteins, human *Mum2* cDNA (NCBI accession number AAD44697) was cloned for expression of GST fusion protein in *E. coli* into the bacterial expression vector pGEX-6P1 using *Bam*HI and *Not*I restriction sites. *E. coli* SCS1 Rosetta cells were transformed with the resulting plasmids and GST-Mum2 was expressed with 1 mM IPTG at 20 °C over night.

Protein was purified with GSH-sepharose according to the batch binding protocol (3.2.5.2) For cleavage of the GST tag elution fractions were incubated with PreScission protease (1:100 w/w) over night at 4 °C. The reaction was then loaded on a HiTrap S cation exchange column equilibrated with 50 mM Tris pH 7.5, 1 mM DTT. Bound Mum2 was eluted with a 0 to 1 M linear NaCl gradient at approximately 0.5 M NaCl. Peak fractions were loaded on a Superdex 75 (16/60) column in 20 mM Tris, pH 7.5, 100 mM NaCl, 2 mM DTT. The elution volume of Mum2 corresponds to the size of a dimer.

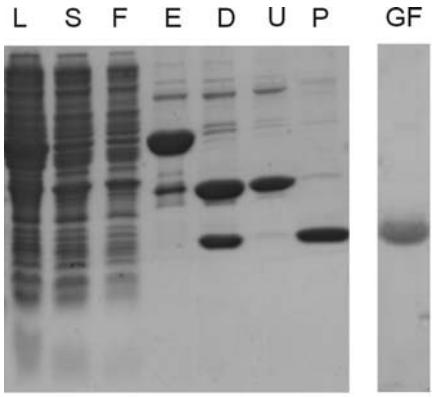

Figure 4.16: SDS-PAGE of samples from the purification of Mum2.
L: total cell lysate; S: soluble supernatant after centrifugation; F: flowthrough after batch binding E: elution from GSH-Sepharose; D: PreScission protease digest; U: unbound fractions from cation exchange chromatography; P: peak fractions from cation exchange chromatography;
GF: purified sample after Superdex 75 gel-filtration;

The Mum2 protein is poorly soluble after removal of the GST-tag. In crystallization trials with Mum2 preparations, only precipitate was obtained, even when protein concentrations as little as 5 mg/ml were used. This was necessary because the protein tended to precipitate at higher concentrations. However, when centrifuged rigorously, the supernatant of such a sample would give a dimer peak when loaded on a gel-filtration column.

To better characterize Mum2, purified samples were investigated with dynamic light scattering (DLS). The spectra shows particle sizes of ~6 nm and 100 nm (Figure 4.17a). The small particles might well represent dimeric protein, but the larger peak indicates aggregates present in solution. Such a polydispers sample is unlikely to yield crystals, and aggregation of Mum2 could not be avoided by changing buffer conditions or the generation of truncated constructs.
In addition, a Fourier transform infrared (FTIR) spectrum of Mum2 was recorded. The presence of two peaks at 1634 cm^{-1} (β-sheet) and 1654 cm^{-1} (α-helix) indicates that Mum2 is at least partially folded (Figure 4.17b).

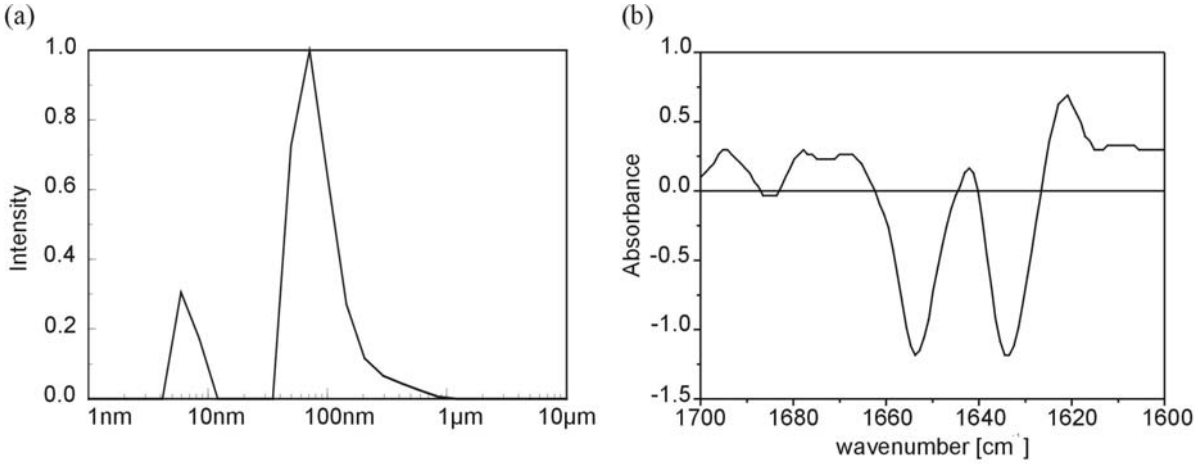

Figure 4.17: (**a**) Representative DLS spectrum of purified Mum2. (**b**) Second derivative FTIR-spectrum of Mum2 recorded at 20 °C.

Similar observations were made when Mum2 was used for nuclear magnetic resonance (NMR) experiment (in collaboration with Christoph Brockmann and Prof. Hartmut Oschkinat, Leibniz-Institut für Molekulare Pharmakologie). The ^{1}H-spectrum of Mum2 and a 2D-HSQC (Heteronuclear Single-Quantum Coherence) spectrum of ^{15}N-labeled Mum2 both indicate that the protein contains some folded parts but is not suitable for structure determination with NMR.

4.5.2 Reconstitution of the Bet3:Tpc6B:Mum2 complex and its interaction with synbindin

The reconstitution of protein complexes can help to stabilize subunits that are poorly soluble when expressed alone. Mum2 was shown to bind to the Bet3:Tpc6B heterodimer (4.3.5, [97]), thus the co-expression of the three proteins was attempted. The *Mum2* gene PCR-amplified with *Bam*HI/*Not*I sites was cloned into the *Bam*HI/*Not*I sites of the bacterial expression vector pET28-KoT that carries a kanamycin resistance. The resulting plasmid was transformed into cells containing pETDuet-*Bet3:Tpc6B* (4.3.1) and transformants were selected for ampicillin and kanamycin resistance.

An overnight culture was inoculated in LB medium containing 100 µg ml^{-1} ampicillin and 30 µg ml^{-1} kanamycin. The pre-culture was diluted 20-fold in the same medium, grown at 37 °C to an OD_{600} of ~0.7 and induced with 1 mM IPTG. Growth was continued for 4 h, cells were harvested by centrifugation, and pellets were stored at -80 °C.

Cells from a 1-liter culture expressing 6×His-Bet3:Tpc6B:Mum2 were purified with Ni-NTA according to the batch binding protocol (3.2.5.1). The elution fraction was loaded on a calibrated Superdex 75 (HiLoad, 26/60) column equilibrated with 20 mM Tris pH 7.4, 200 mM NaCl and 2 mM DTT (Figure 4.18b). A high molecular-weight peak with a elution volume corresponding ~120 kDa is observed, that contained all three proteins. Considering the molecular weight of the individual subunits, the complex is likely to represent a dimer of His-Bet3:Tpc6B:Mum2 heterotrimers: one Mum2 homodimer (as described in 4.5.1) probably links two Bet3:Tpc6B heterodimers. In addtion, a low molecular-weight peak was observed at an elution volume corresponding to 40 kDa. In these fractions only Bet3 was found, suggesting the presence of excess Bet3 homodimers from the co-expression.

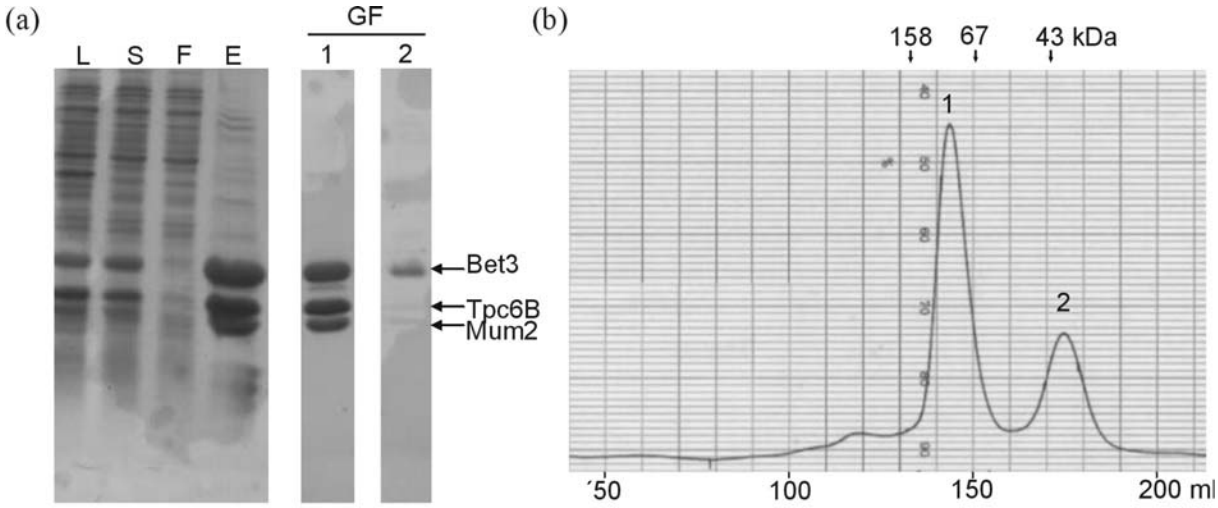

Figure 4.18: (**a**) SDS-PAGE of samples from the purification of His-Bet3:Tpc6B:Mum2.
L: total cell lysate; S: soluble supernatant after centrifugation; F: flowthrough after batch binding; E: elution from Ni-NTA agarose; GF: peak fractions 1 and 2 from Superdex 75 gel-filtration.
(**b**) Chromatogram from Superdex 75 (HiLoad, 26/60) gel-filtration. A high-molecular weight (1, 120 kDa) and a low-molecular weight peak (2, 40 kDa) are separated.

The purified complex was included in crystallization trials, but no crystals could be obtained. Furthermore it is questionable whether the isolated hexamer represents a TRAPP subcomplex. Bet3 and Tpc6 are present as homodimers when expressed alone, but upon co-expression the heterodimer is formed. Thus, Mum2 might also heterodimerize if the appropriate TRAPP subunit is co-expressed instead of promoting the formation of a hexamer *via* its homodimerization. A pulldown assay was used to identify that putative binding partner of the His-Bet3:Tpc6B:Mum2 complex that took advantage of the affinity tag of Bet3. Indeed, when

incubated with HEK293 cell lysates expressing flag-synbindin, a specific interaction between the proteins can be detected (Figure 4.19).

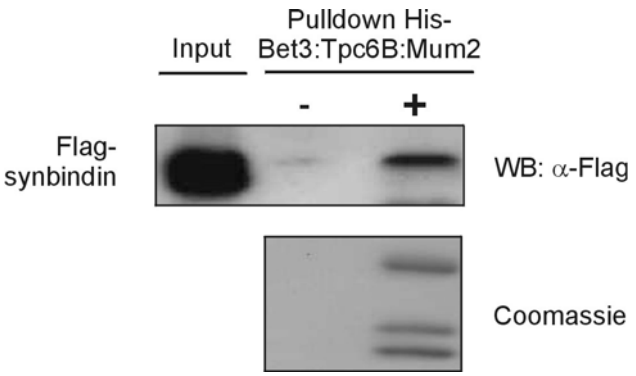

Figure 4.19: Pulldown assay with His-Bet3:Tpc6B:Mum2. A specific interaction with flag-synbindin expressed in HEK293 is observed.

4.5.3 Purification and crystallization of the Bet3:Tpc6B:Mum2:synbindin complex

For the co-expression of the four TRAPP subunits the pQLink system was used [68]. Bet3, Tpc6B, Mum2, and synbindin were cloned into pQLinkH and the resulting plasmids were used to first construct a co-expression plasmid of the subunits Bet3 and Tpc6B (pQLinkH-*Bet3:Tpc6B*). Then Mum2 was included in the plasmid (pQLinkH-*Bet3:Tpc6B:Mum2*) and finally a plasmid with all four subunits, including synbindin, was constructed (pQLinkH-*Bet3:Tpc6B:Mum2:synbindin*). All proteins were expressed as fusion proteins with a 6xHis-tag cleavable with TEV protease.

With expression constructs containing up to four subunits in hands, the assembly and stoichiometry of the TRAPP subcomplexes could be adressed. Combinations of Bet3:Tpc6B, Bet3:Tpc6B:Mum2 and Bet3:Tpc6B:Mum2:synbindin were expressed in 0.5 l Overnight Express Instant TB medium supplemented with 100 µg ml^{-1} ampicillin over night. Cells were lysed with a French Press and purified using Ni-NTA agarose as described (4.2.5.1). Elution fractions from affinity chromatography were applied on a Superdex 200 26/60 gel-filtration column equilibrated with 20 mM Tris pH 7.5, 200 mM NaCl, 2 mM DTT (Figure 4.20a). The isolated TRAPP subcomplexes were analyzed with SDS-PAGE, showing the formation of two-, three- and four-protein complexes (Figure 4.20b). As described before (4.3.1), Bet3 and Tpc6B form a 40 kDa heterodimer, which binds Mum2. The isolated Bet3:Tpc6B:Mum2 complex shows a molecular weight of ~90 kDa, indicating the binding of a Mum2 dimer. This is consistent with the finding that Mum2 binds as homodimer (4.5.2), however, the formation of dimers of trimers is not observed. This might be due to the different expression systems used. All subunits contain a 3 kDa terminal sequence (TEV cleavage site and His-tag) in

pQLinkH, which might lead to some sterical hindrance, but Tpc6B and Mum2 did not contain any tag in pETDuet-1 and pET-28 KoT. Including synbindin in the co-expression system led to the formation of a complex of similar size. Thus, a Mum2:synbindin heterodimer instead of a Mum2 homodimer is likely to bind to Bet3:Tpc6 during complex assembly (Figure 4.20c).

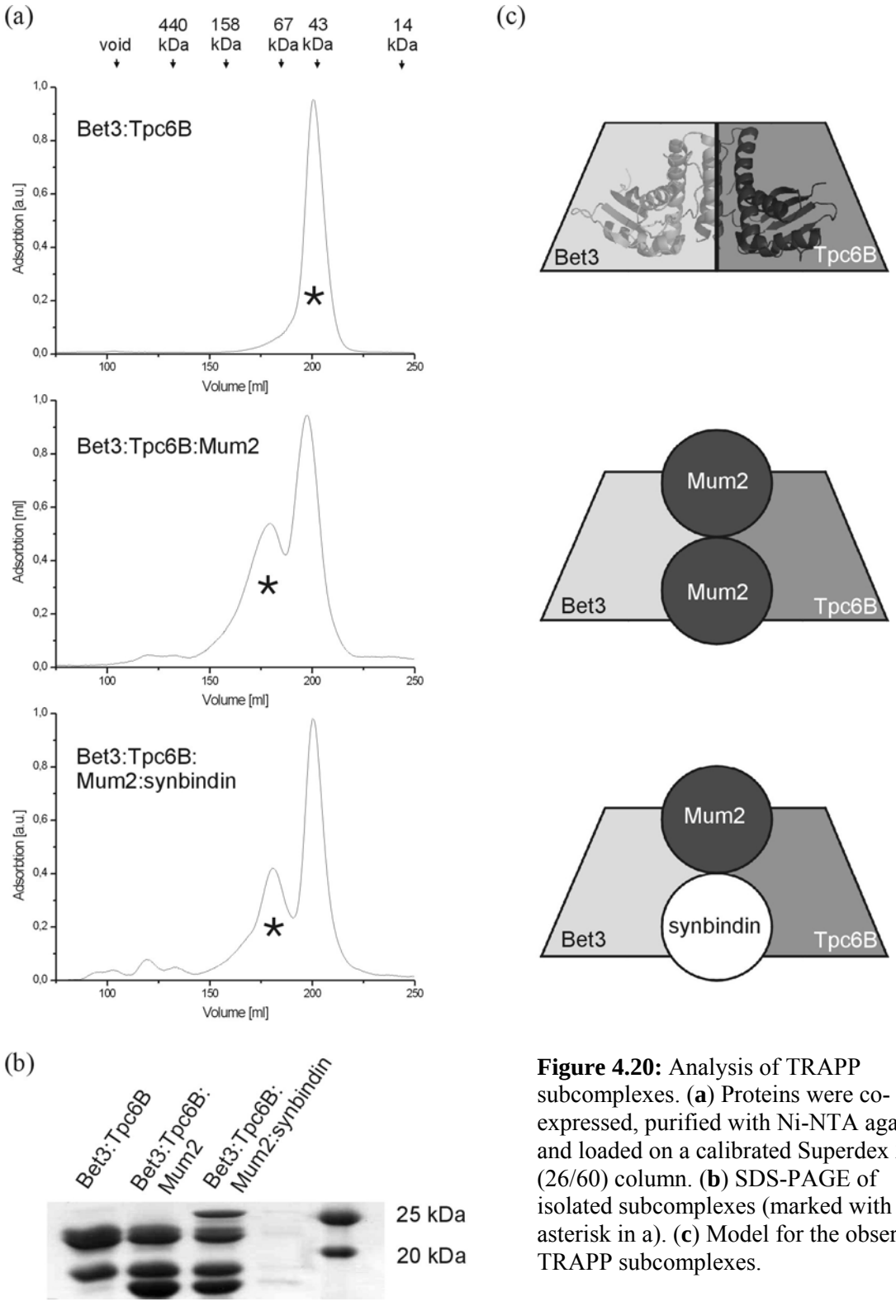

Figure 4.20: Analysis of TRAPP subcomplexes. (**a**) Proteins were co-expressed, purified with Ni-NTA agarose and loaded on a calibrated Superdex 200 (26/60) column. (**b**) SDS-PAGE of isolated subcomplexes (marked with an asterisk in a). (**c**) Model for the observed TRAPP subcomplexes.

This tetrameric complex could be expressed and purified on a large scale according to the protocol described in 4.6.2. The high-molecular weight fractions were pooled and dialyzed against 20 mM Tris pH 7.5, 200 mM NaCl, 2 mM DTT, 10 mM EDTA. The protein was concentrated to 3 mg ml^{-1} and used for crystallization in 96-well format at 20 ºC by the sitting-drop method with a semi-automated dispensing system [74]. Reservoir volume was 400 µl and the droplet contained 400 nl of each protein solution and precipitant. Best crystals from initial refinement were obtained in 4-5% PEG 3350, 0.1 M MES pH 5.5 precipitant solution. Crystals were transferred into cryo-solution containing additional 20% 2,3-butanediol or 25% ethyleneglycol and flash-frozen in liquid nitrogen. Diffraction to 6 Å was observed at BESSY [76].

Figure 4.21: Crystal of the Bet3:Tpc6B:Mum2:synbindin complex, grown in 4% PEG 3350, 0.1 M MES pH 5.5

4.6 Palmitoylation of Bet3

The most striking feature of the crystal structure of Bet3 [56, 57] is the presence of a palmitoyl group, located in a hydrophobic tunnel in the interior of the protein and covalently linked *via* a thioester-bond to a cysteine residue conserved from yeast to man. Bet3 was also palmitoylated in the crystal structures of the Bet3:Tpc6 complexes ([97, 99], 4.3.4) (Figure 4.25b). This and the conserved nature of the palmitoylation site points towards an important function for Bet3 palmitoylation that remains to be elucidated. Some of the experiments presented in this chapter were done in collaboration with PD Dr. M. Veit from the Free University Berlin [100]. This applies to Figures 4.24, 4.25a and 4.26b.

4.6.1 Palmitoylation is not required for membrane association of Bet3 or yeast cell viability

Initial studies on the palmitoylation of Bet3 were carried out in yeast, using the plasmid pYEXTHS-BN-*Bet3*, coding for human Bet3 (see 4.2.1). The yeast *BET3* gene YKR068c was PCR amplified from AH22*ura*3 genomic DNA and cloned accordingly into the vector pYEXTHS-BN. Of both constructs, the conserved palmitoylation site was mutated from cysteine to serine, resulting in the expression of Bet3 C68S (human) and Bet3p C80S (yeast protein).

Palmitoylation of cysteine residues is a natural modification, but can also be forced under unphysiological conditions. To test whether Bet3 palmitoylation occurs *in vivo* or might be an artifact of protein purification, metabolic labeling of yeast cells with ^{3}[H]-palmitate was carried out. In cultures expressing wild-type Bet3 and Bet3p precipitated protein was palmitoylated as shown by fluorography. In contrast no palmitic acid was attached to the CS mutant proteins (Figure 4.22). Differences in intensity between human and yeast protein are due to the higher expression level of Bet3 compared to Bet3p.

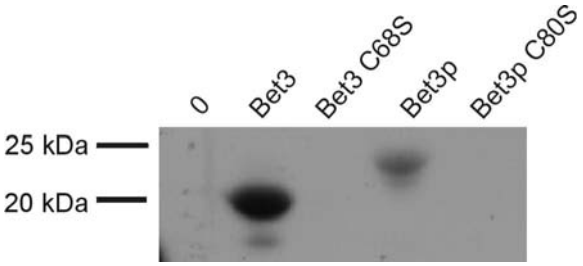

Figure 4.22: Metabolic labeling with [^{3}H]-palmitate. Yeast cells with and without Bet3 plasmids were grown in the presence of [^{3}H]-palmitic acid. Bet3 and Bet3p are labeled at equivalent sites as shown by SDS–PAGE and fluorography.

Previous studies have shown that membrane-bound Bet3p resides on the *cis*-Golgi complex [33]. Thus, the question was adressed if Bet3 palmitoylation is involved in its membrane anchoring. Preparations of cytosolic and membrane fractions from yeast cells expressing Bet3 and Bet3 C68S, respectively, were analyzed with immunoblotting. It can be shown that wild-type and mutant Bet3 are localized in the cytosol and on the membrane (Figure 4.23a). Membrane association of Bet3 could also be shown when crude cell lysates from Bet3 expressing yeast cells was loaded on a sucrose cushion. Here the protein was found in the microsomal fractions and did not precipitate as aggregates, demonstrating that Bet3 actually is membrane-associated and not aggregated. In the membrane extractions, both proteins are resistant to extraction with high salt, urea, carbonate and Triton X-100, a feature characteristic for tightly membrane associated proteins (Figure 4.23b). The integral membrane protein Sec61p and the peripheral membrane-associated proteins Cdc48p and Ubc7p served as references in these experiments. These data show that Bet3 is tightly bound to membranes, but that this interaction does not require palmitoylation. This suggests that the tight binding to an anchor protein or another modification are necessary to mediate the membrane association of Bet3.

The question remains if palmitoylation of Bet3 is essential for protein function *in vivo*. Bet3 constructs were transformed in a yeast *bet3* deletion strain (Y25984) and sporulation of these transformants was induced. Loss of Bet3p is lethal leading to only two viable spores in tetrad analysis if no complementation can be achieved through the transformed constructs. Bet3 is not able to rescue haploid cells with a *bet3* deletion despite showing high level of sequence homology, but both Bet3p and Bet3p C80S can (Figure 4.23c). Thus, palmitoylation of Bet3p does not appear to be essential for the physiological function. However, the expression of Bet3p under the control of a copper promotor, even when not induced, might lead to a high intracellular level of Bet3p. A fine-regulatory effect of the palmitoylation on protein stabilization or modulation of protein-protein interaction can therefore probably not be detected in this system.

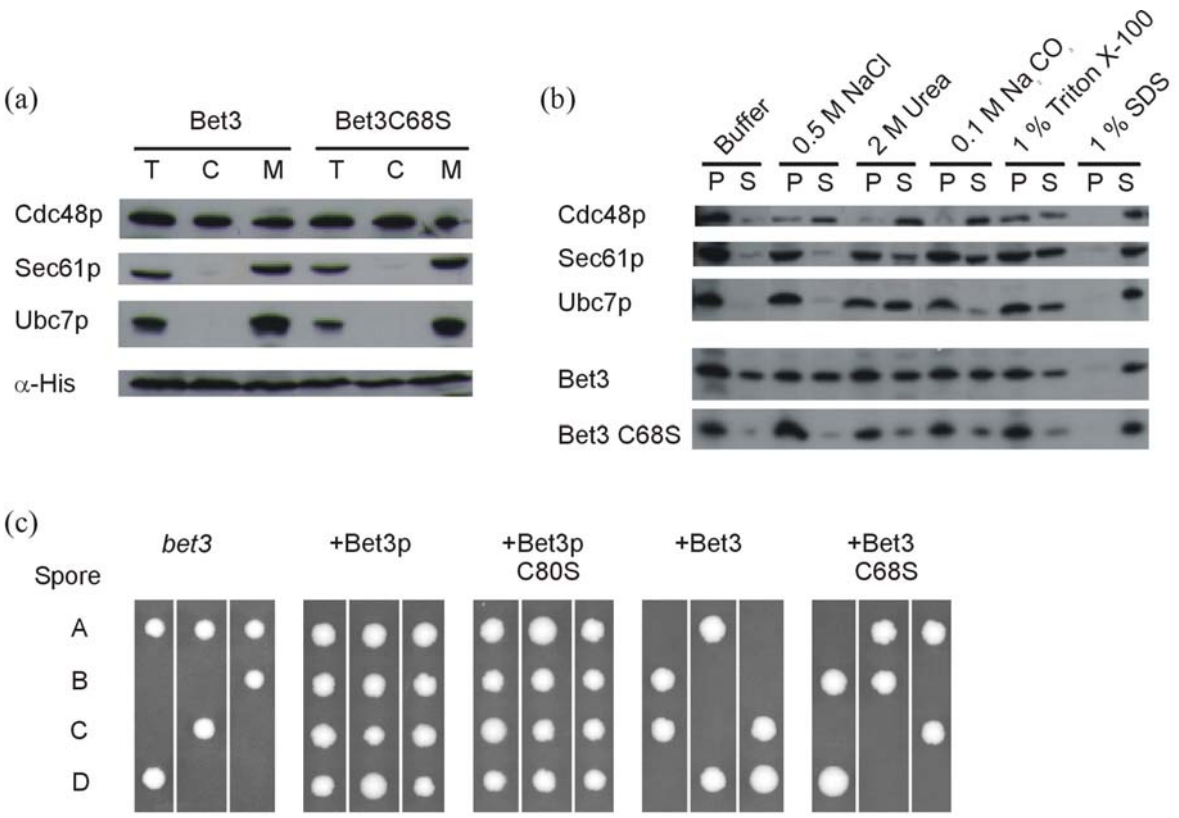

Figure 4.23: (**a**) Membrane preparations from yeast expressing Bet3 and Bet3 C68S. Cleared total cell lysates (T) were subjected to ultracentrifugation and separated into cytosolic (C) and microsomal (M, 10-fold concentrated) fractions. Wild-type and mutant protein bind to the membranes. (**b**) Membrane extractions of Bet3 and Bet3 C68S. Membranes were treated with buffer, 0.5 M NaCl, 2 M urea, 0.1 M Na_2CO_3, 1% Triton X-100 or 1% SDS and subsequently separated into pellet (P) and supernatant (S) fractions by centrifugation. (**c**) Tetrad analysis of yeast Y25984 *bet3* deletion strain. Sporulation was induced in cells with and without Bet3 plasmids, and spores were dissected on YPD plates of individual tetrads.

4.6.2 Bet3 possesses strong auto-palmitoylation activity

It was surprising that Bet3 was found to be palmitoylated, even if the recombinant protein used for purification was expressed in *E. coli*, which lack enzymes for acylation of proteins [56, 57]. This indicates that Bet3 might be able to mediate its own palmitoylation.

To test whether Bet3 has self-palmitoylating activity, recombinant Bet3 from yeast was purified as described before (4.2.1) and used in an *in vitro* palmitoylation assay performed by Dr. M. Veit. Protein was incubated with [^{3}H]-palmitoyl-CoA for 30 min at 30 °C and the reaction was subjected to chloroform/methanol precipitation, SDS-PAGE, staining with Coomassie and fluorography. The assay was carried over a pH range from 5.5 to 12.5, showing that palmitoylation of Bet3 has a broad pH optimum at neutral pH, but is completely inhibited at acidic pH and reduced at basic pH (Figure 4.24a). The palmitoylated cysteine has to act as a strong nucleophile in the nucleophilic attack for acyl transfer and should therefore be present in its deprotonated form. Thus spontaneous acylation should be characterized by a linear increase in the palmitoylation efficiency when plotted against the pH [101]. This is not

observed for Bet3, indicating specificity of the reaction and a pH optimum corresponding to physiological conditions. The residual labeling at basic pH may be due to acylation at irrelevant sites. The labeling of Bet3 in the palmitoylation assay was very efficient and much stronger than for other palmitoylated proteins from the literature [102]. To determine the Pal-CoA concentration at which the rate of Bet3 palmitoylation is most efficient, Bet3 was incubated for 5 min with increasing amounts of [^{3}H]-Pal-CoA (Figure 4.24b). Quantification of the fluorogram shows that the reaction begins to saturate at 10 µM Pal-CoA. Analysis of these data according to Michaelis-Menten ($v = v_{max} \times [S] / K_m + [S]$) yielded a pseudo-$K_m$ of Bet3 for Pal-CoA of 5.7 µM. Although the Michaelis-Menten equation might not be accurate for a reaction in which the enzyme is used up the data nevertheless indicate that palmitoylation of Bet3 occurs in the range reported for Pal-CoA concentrations inside cells (5-160 µM [103]).

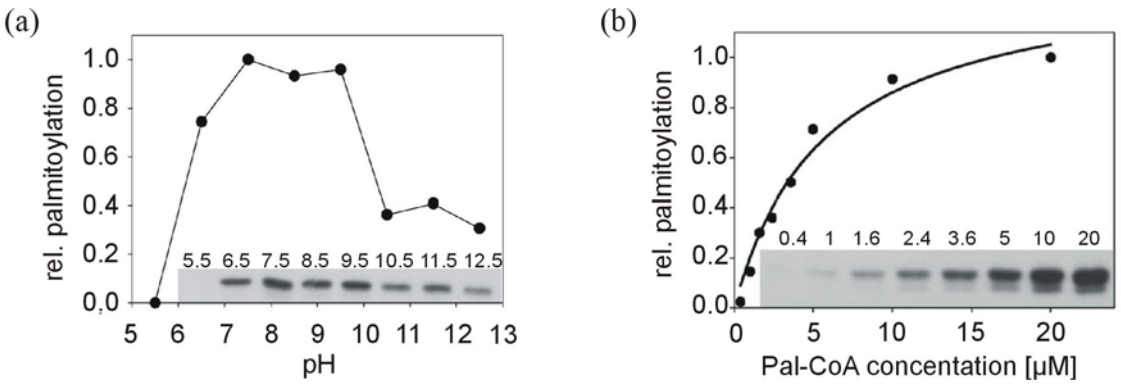

Figure 4.24: (**a**) Bet3 was incubated with [^{3}H]-Pal-CoA at different pH as indicated. The resulting fluorogram (inset) was quantified and relative palmitoylation is plotted against the pH. (**b**) Bet3 (2 µM) was incubated with increasing concentrations of [^{3}H]-Pal-CoA for 5 minutes at 30 °C. The resulting fluorogram (inset) was quantified and the relative palmitoylation was plotted against the [^{3}H]-Pal-CoA concentration. The data points were fitted according to the Michaelis-Menten equation.
Palmitoylation assays and fluorography were performed by Dr. M. Veit.

To elucidate the mechanism of Bet3 palmitoylation, several mutants of Bet3 were produced (Table 4.7). To overcome solubility problems with some of the mutants, human *Bet3* cDNA was cloned into the bacterial expression vector pGEX-4T1 for expression of GST fusion protein in *E. coli*. Site directed mutagenesis was performed according to a QuikChange mutagenesis protocol. *E. coli* BL21 (DE3) cells were transformed with the resulting plasmids. GST-Bet3 was purified with the batch binding method and elution fractions were dialyzed against 25 mM Tris, pH 8.4, 120 mM NaCl.

The effect of the mutations on the auto-palmitoylation of Bet3 was adressed with palmitoylation assays carried out by Dr. M. Veit.

Bet3	proposed effect
wt	-
C68S	not palmitoylated [56, 57]
C68A	not palmitoylated
A82L	channel blocking [56]
A82V	channel blocking
R67E	less nucleophilic cysteine 68

Table 4.7: List of GST-Bet3 fusion proteins used in this study. For the different Bet3 mutants the expected effect on protein structure or function is given.

Exchange of cysteine 68 by serine or by alanine almost completely inhibited [^{3}H]-palmitate labeling of Bet3 (Figure 4.25a). Thus, self-palmitoylation of Bet3 occurs at cysteine 68. The acylation of Bet3 *in vitro* might require an open hydrophobic tunnel that can bind the palmitoyl moiety of Pal-CoA. The replacement of alanine 82 in the middle of the tunnel by a bulkier amino acids such as valine narrows the pocket such that it can no longer accommodate a hydrocarbon chain (Figure 4.25b). Acylation of Bet3 A82V and of A82L is marginal (Figure 4.25a), indicating that the fatty acid must insert into the tunnel to become stably attached. Multiple sequence alignment of Bet3 sequences showed adjacent to the palmitoylated cysteine an arginine, which is completely conserved from yeast to man. Basic amino acids in the vicinity of palmitoylated cysteines often affect the acylation reaction, probably by decreasing the pK_a of the cysteine´s SH group [60, 104, 105]. Replacing arginine 67 by glutamic acid almost completely blocked palmitoylation of Bet3, arguing for a role of this residue in the acylation reaction.

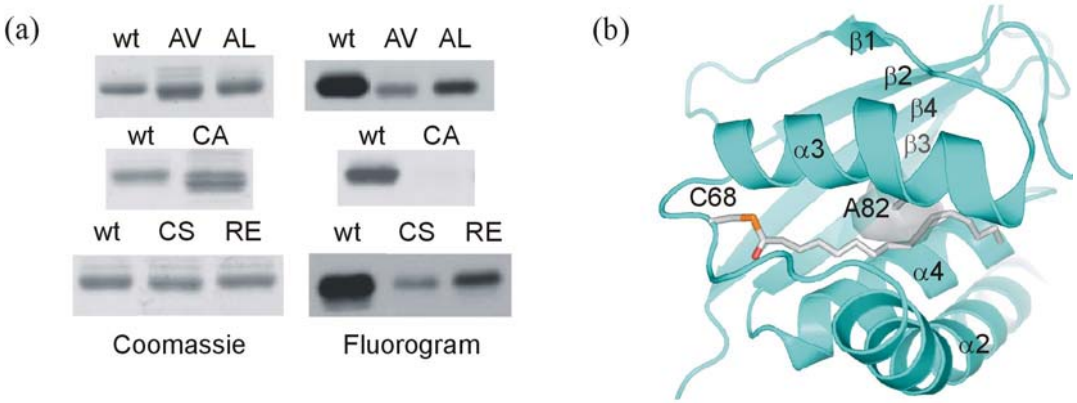

Figure 4.25: (**a**) Similar amounts of GST-Bet3 wild-type (wt), C68S, C68A, A82V, A82L and R67E were incubated with [^{3}H]-Pal-CoA. The left part of the figure shows the Coomassie-stained gel, the right part the fluorogram. (**b**) View of the hydrophobic tunnel of Bet3 with buried palmitoyl group. Secondary structure elements and Cys 68 carrying the covalent modification are labeled. Ala 82 is shown in stick representation and the modeled channel-blocking mutation to valine is drawn as semitransparent surface.
Palmitoylation assays and fluorography were performed by Dr. M. Veit.

4.6.3 Palmitoylation is required for Bet3 protein stability *in vitro* and *in vivo*

Those mutant Bet3 proteins lacking efficient self-palmitoylation activity were harder to express in *E. coli*, and recombinant proteins were unstable after cleavage of the GST-tag. It is also striking that in all crystal structures determined to date Bet3 was found to be palmitoylated, indicating that the fatty acid has a beneficial effect on the structure of the protein [56, 57, 97, 106]. The difference in protein stability was quantitatively determined between acylated Bet3 and Bet3 gently depalmitoylated with hydroxylamine. Temperature melting curves of both samples were measured with circular dichroism (CD) spectroscopy by recording the decrease in ellipticity at 222 nm upon heating of protein samples. Both proteins revealed similar CD spectra in the beginning, indicating that both proteins had similar secondary structure compositions at low temperature. However, unfolding of deacylated Bet3 starts at lower temperature than unfolding of native, palmitoylated Bet3 (Figure 4.26a). The melting temperatures differ by 10 °C, proving a significant decrease in protein stability upon loss of palmitoylation. The lack of a ligand in the hydrophobic tunnel might lead to a partial misfolding which destabilizes of the protein. At high temperatures both acylated and non-acylated Bet3 are not completely unfolded but form β-aggregates, as seen in the absence of a plateau in the melting curves and characteristic CD spectra of heated samples.

Pulse-chase experiments were carried out (by Dr. M. Veit) to detect effects of palmitoylation on the stability of Bet3 *in vivo*. BHK cells were transfected with plasmids encoding acylated and non-acylated Bet3 and incubated for 24 h to allow expression of the protein. Protein synthesis was then blocked and cells were incubated further for 5, 20 and 44 h prior to analyzing the remaining amount of Bet3 in cellular extracts by blotting. Whereas palmitoylated Bet3 is stable for at least 44 h, the amount of the non-acylated mutants A82V and C68A decreased rapidly after 5 h of incubation (Figure 4.26b).

If non-palmitoylated Bet3 adopts a different tertiary structure than the palmitoylated form *in vivo* one would expect that protein-protein interactions of Bet3 are impaired. Thus, the binding of Bet3 A82V and C68A to Tpc6B was tested. In co-immunoprecipitation experiments with transfected HEK293 cells, binding of Bet3 mutants to Tpc6B was almost completely abolished (Figure 4.26). Since the mutation sites of unpalmitoylated Bet3 (A82V and C68A) are spatially far apart from its interaction interface with Tpc6B, a profound change in the tertiary arrangement must have occurred.

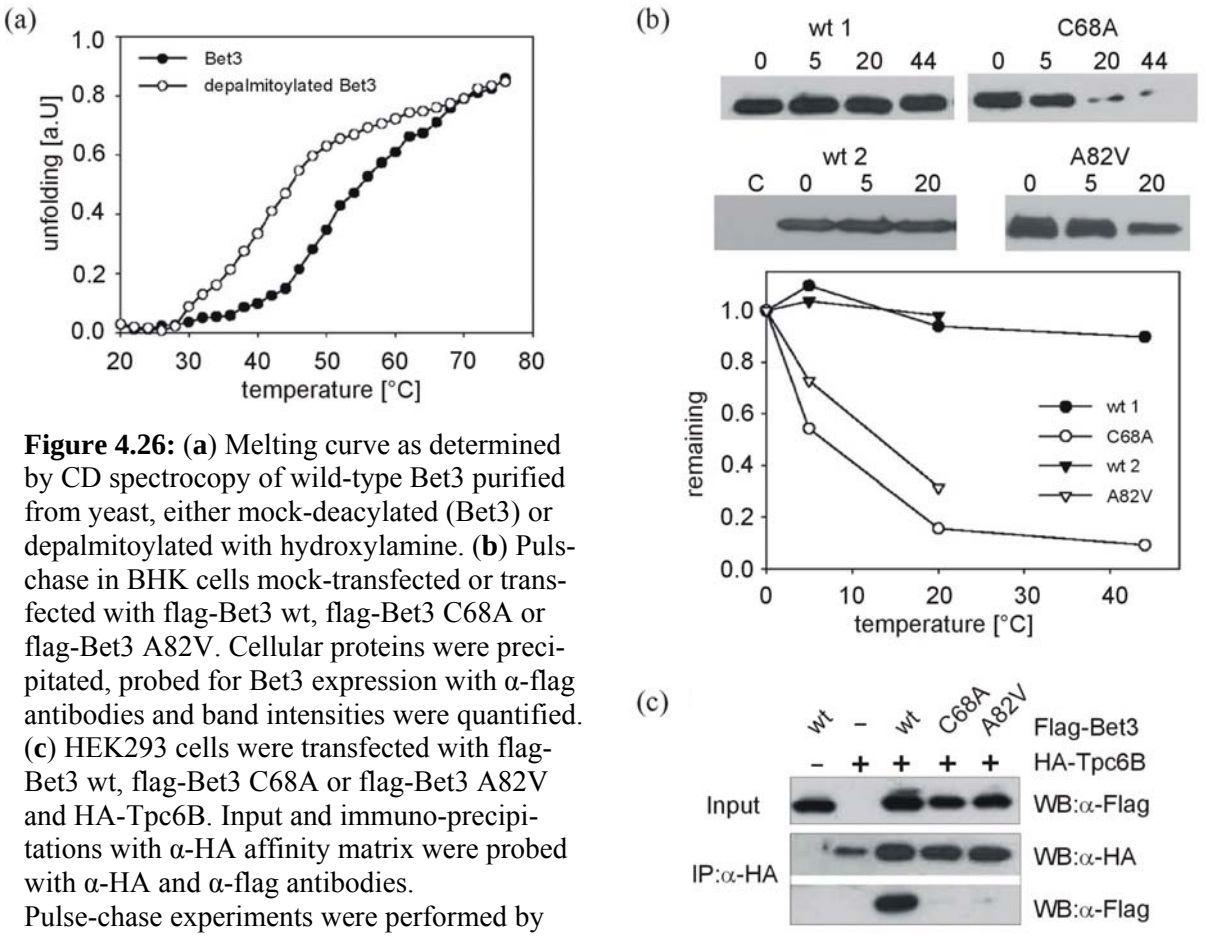

Figure 4.26: (**a**) Melting curve as determined by CD spectrocopy of wild-type Bet3 purified from yeast, either mock-deacylated (Bet3) or depalmitoylated with hydroxylamine. (**b**) Puls-chase in BHK cells mock-transfected or trans-fected with flag-Bet3 wt, flag-Bet3 C68A or flag-Bet3 A82V. Cellular proteins were preci-pitated, probed for Bet3 expression with α-flag antibodies and band intensities were quantified. (**c**) HEK293 cells were transfected with flag-Bet3 wt, flag-Bet3 C68A or flag-Bet3 A82V and HA-Tpc6B. Input and immuno-precipi-tations with α-HA affinity matrix were probed with α-HA and α-flag antibodies.
Pulse-chase experiments were performed by Dr. M. Veit.